



# Cross-hole Seismic Field Experiments and Imaging for Karst Caves in Deep Foundations

Chenglong Duan\*, Changhong Yan, Baotian Xu, and Yinkang Zhou  
School of Earth Sciences and Engineering  
Nanjing University, China  
[\\*clduan@itasca.cn](mailto:clduan@itasca.cn)



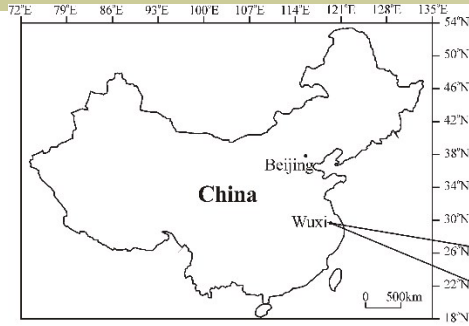
# Outline



- Background and methodology
- Field data acquisition
- Seismic imaging (CT) technique
- Results and interpretations
- Conclusions



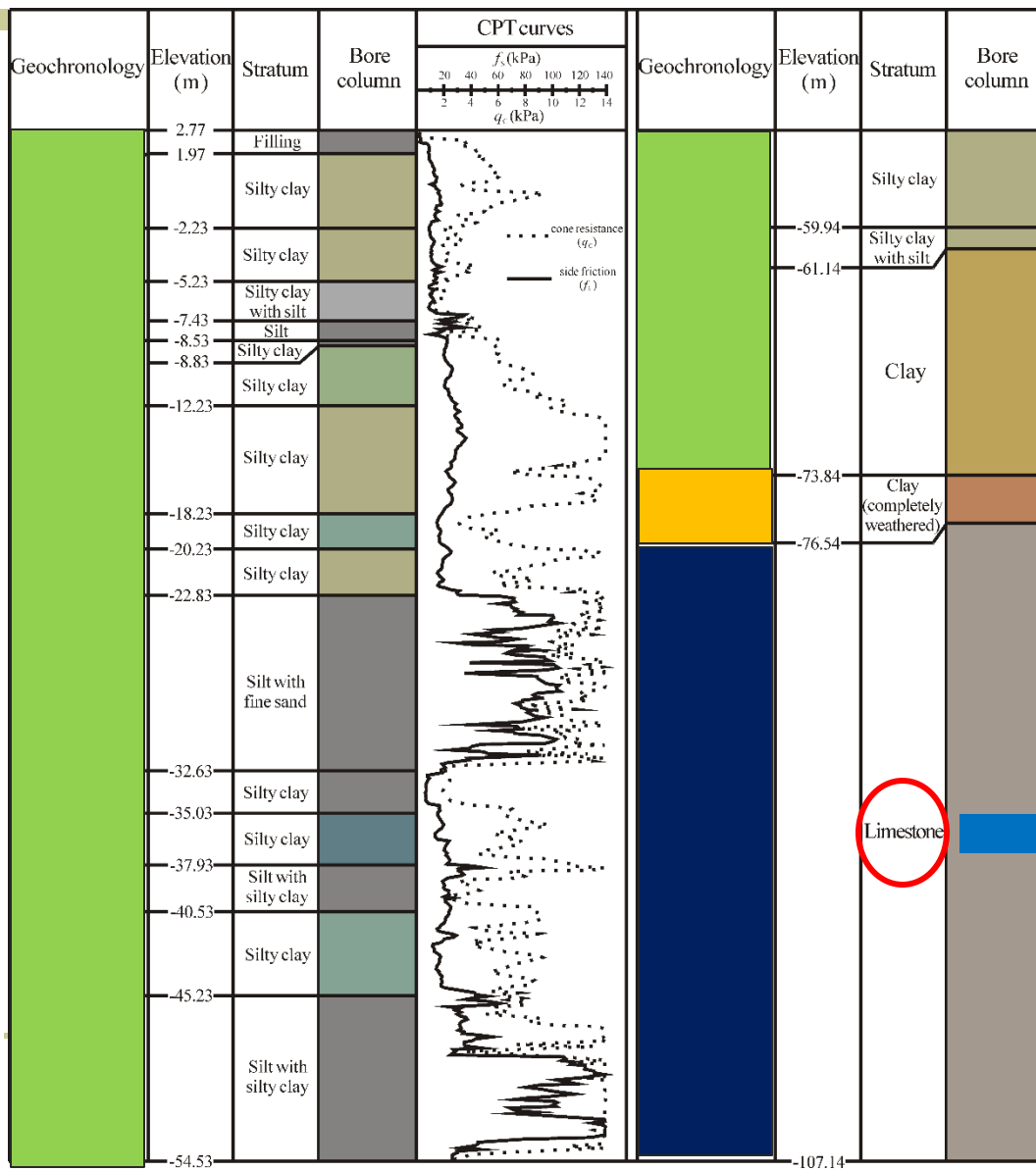
# Background---Problem introduction



- Foundation type:  $\Phi 1000$  mm drilled grouting pile
- Pile length:  $\sim 75$  m
- Pile-end requirement: moderately weathered to un-weathered bedrock



# Background---Problem introduction



Triassic Qinglong formation  
( $T_{1x}$ ) limestone  
(76.54-107.14 m, without penetration)

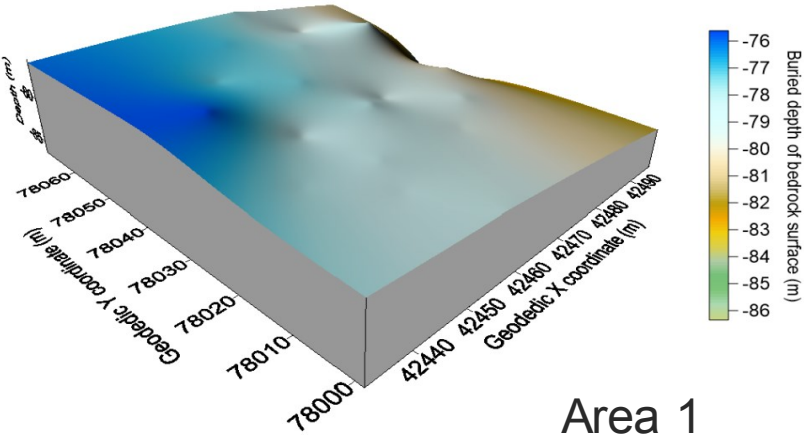




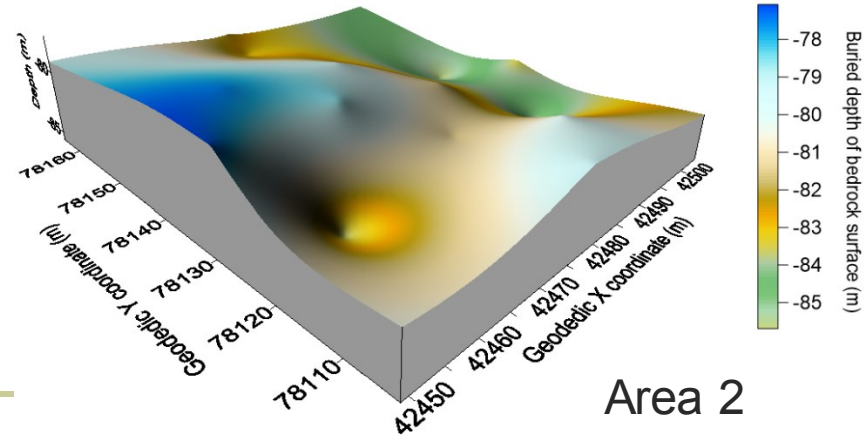
# Evidence for the development of karst



- Highly-developed limestone fractures, mainly horizontal or slow angles
- Dip direction of the strata: SW / Dip: 10-25°
- Undulating bedrock surface → uneven terrain before being covered during the Quaternary



Area 1



Area 2



# Evidence for the development of karst



- Corrosive CO<sub>2</sub> was abundant (11.65 mg/L on average)
- Low-lying recharge area for karst-fracture groundwater with moderate water flow



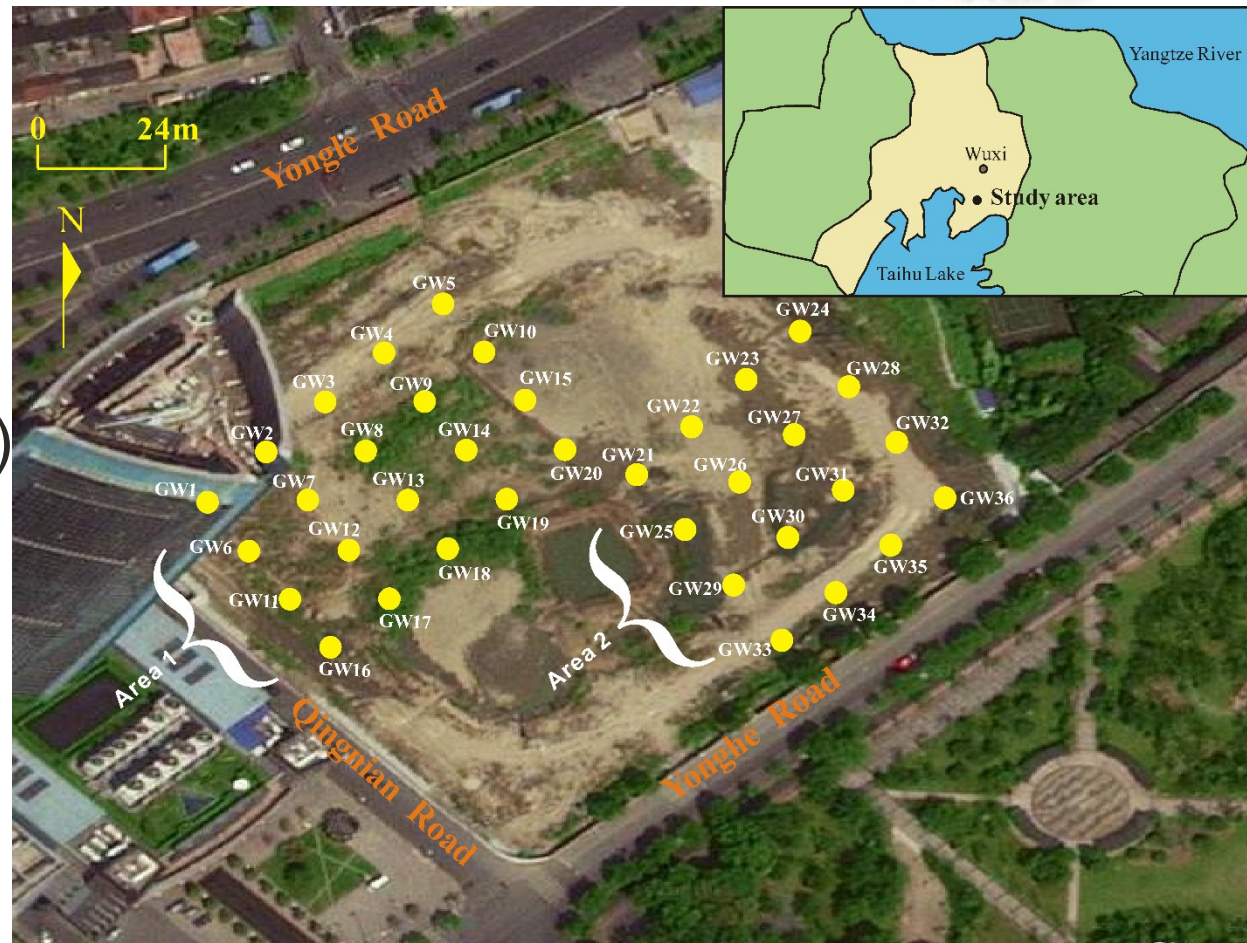
Groundwater circulation was active and played a dominant role in karst processes in this area.



# Results of borehole survey



- 36 boreholes
- Cave properties  
(77.0-100.1 m):  
mean=1.52 m,  
max=8.0 m(GW36)  
cohesive soil  
/ gravel filled





# Results of borehole survey



- 36 boreholes
- Cave properties  
(77.0-100.1 m):  
mean=1.52 m,  
max=8.0 m(GW36)  
cohesive soil  
/ gravel filled

Intensively developed



Intensively developed



# Results of borehole survey



- 8 supplementary boreholes
- 11 karst caves with a mean diameter of 1.76 m

Karst caves were found in 31/44 (70.5%) boreholes.

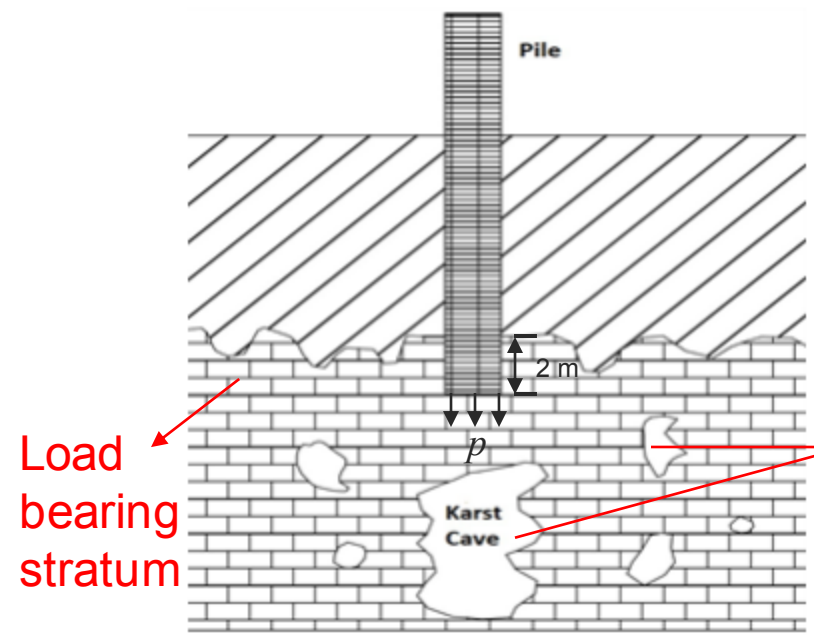




# Problem generation



- Karst caves greatly impact the pile bearing capacity.
- For the sake of safety, the positions, sizes and filling types of the karst caves have to be **investigated**.



(After Gao *et al.*, 2014)

Effective means of detection ?  
Insightful data analysis ?

1. Deep-buried;
2. Wide distribution;
3. Local large scale



# Detection method



	Deep-buried	Wide distribution	Local large scale
■ Near surface (Nondestructive) methods (GPR, ERT, Seismic refraction tomography, Ultrasonic tomography...)			
■ Borehole survey			
■ Cross-hole seismic CT			



# Background---Research status



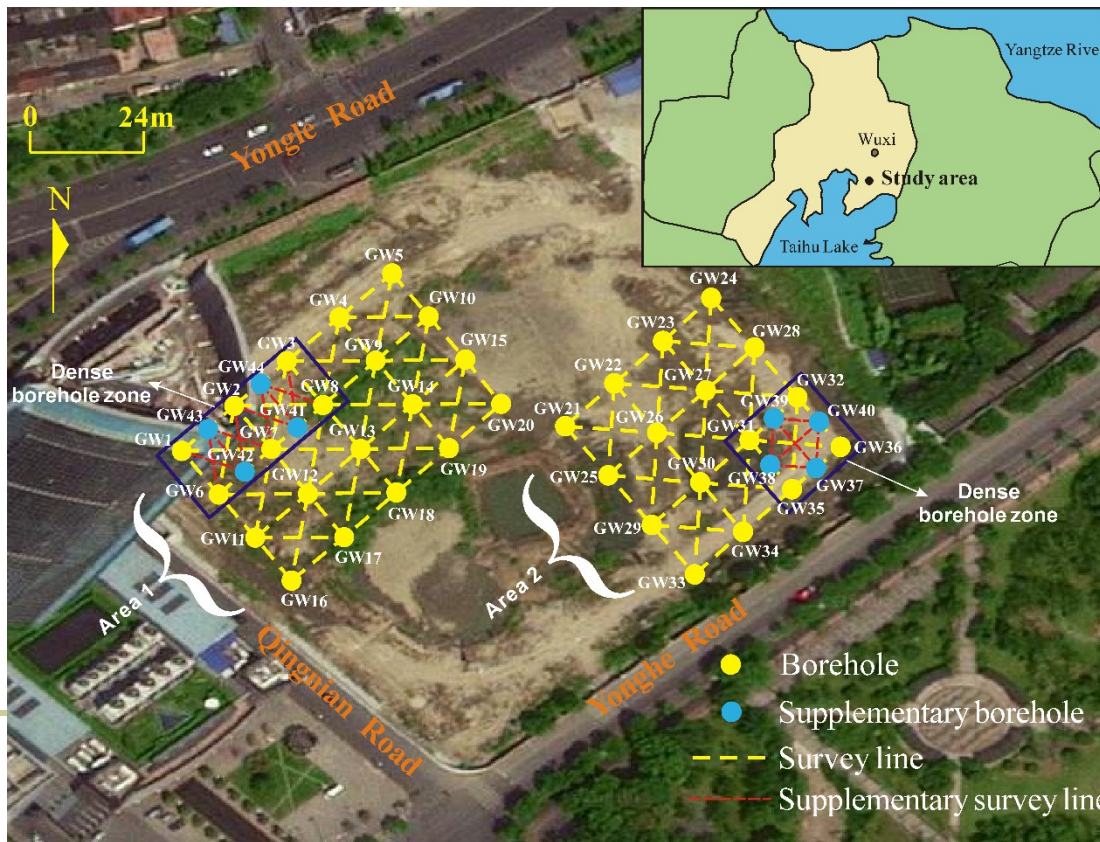
Data sources: cnki (in Chinese); ScienceDirect (in English)

- Most are shallow problems (karst, aquifers, fracture rockmass...), few studies addressed detections on deep karst foundations.
- • Data processing problems • Narrow and simple approaches • Multiple interpretation results • Practice > theory



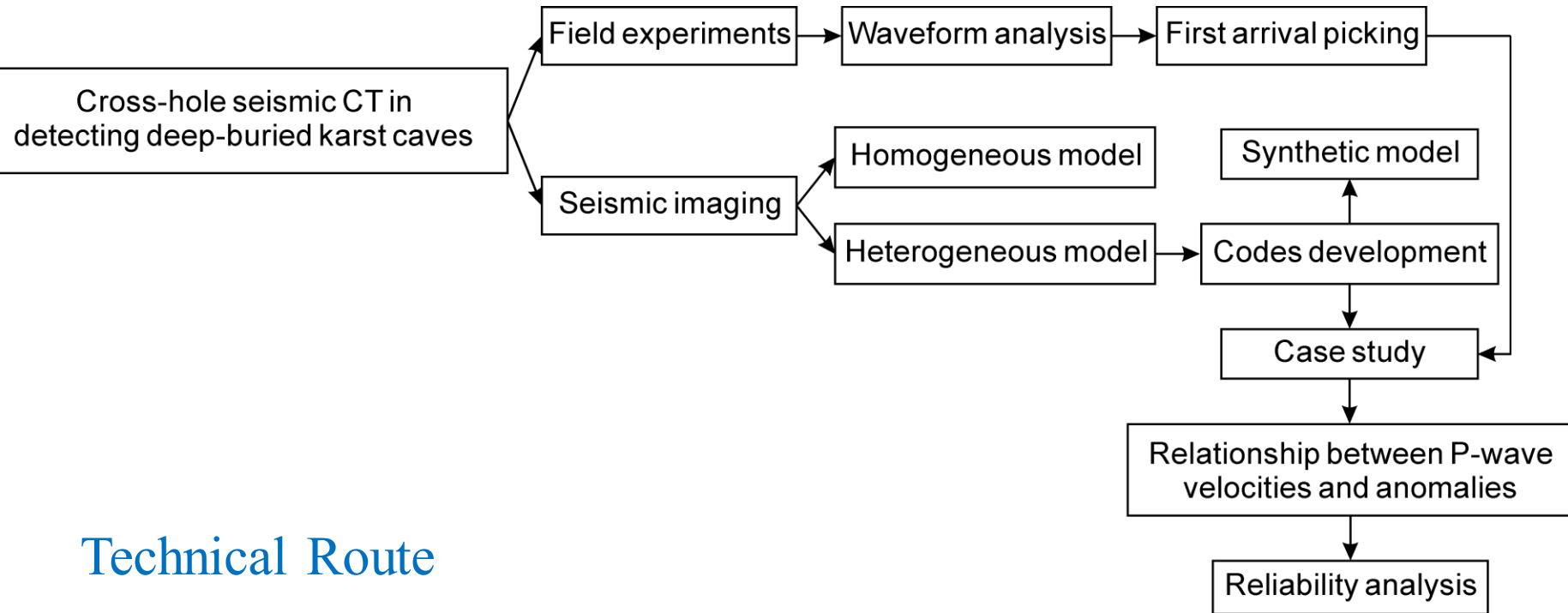
# Methodology

- 113 total survey lines (63 in Area 1 and 50 in Area 2)
- The length of each survey line varied from 12.0 m to 18.5 m.





# Methodology



## Technical Route



# Field data acquisition



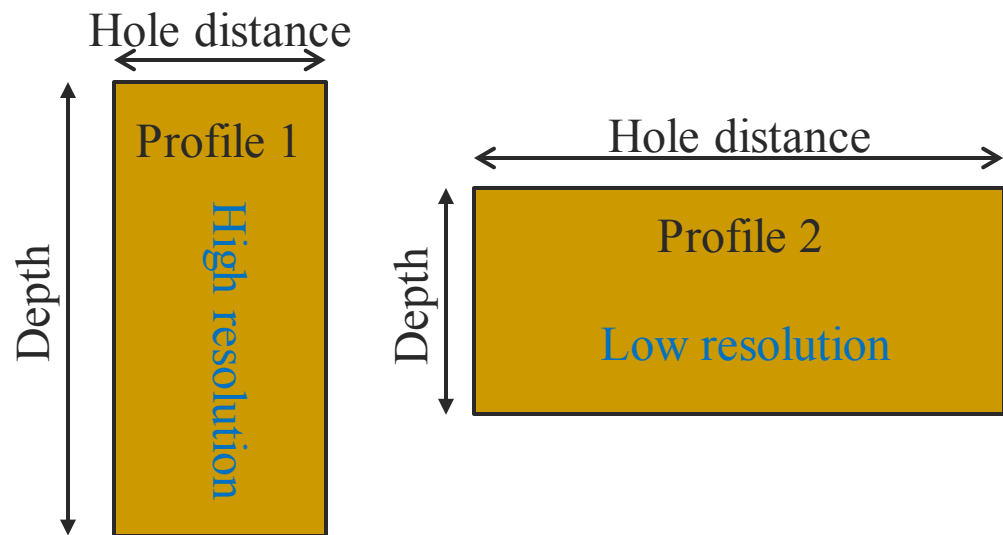
- Detection targets
  - Profile: more than 12 m below the bedrock
  - Depth: more than 75 m from surface
- Technical difficulties:
  - Entry and exit of detecting probes
  - Thick overlying soil
  - Avoid tube waves
- Requirements



# Field data acquisition



- Max distance between two boreholes → < 30 m
  - Ray cover density
    - \* collection interval → 0.5 m
    - \* profile design
  - Record delay → zero
  - Central frequency
- ↓
- 60Hz, 100Hz**

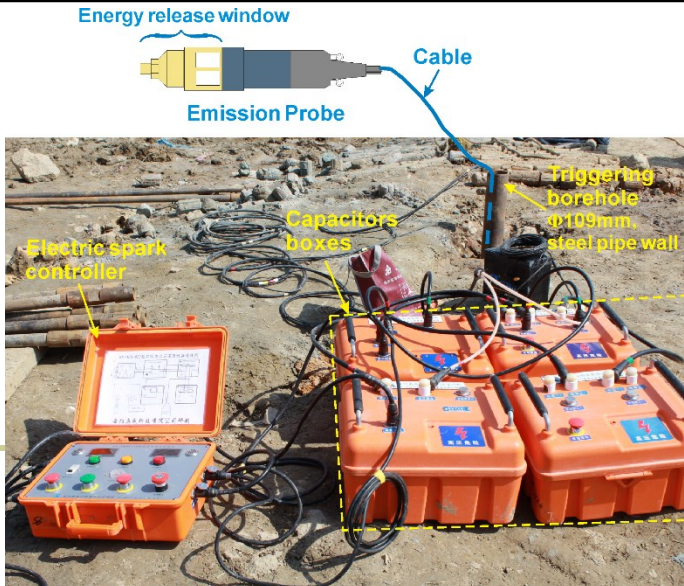




# Field data acquisition



Test apparatus	Manufacturer	Parameters for acquisition
Electric spark source (HX-DHH-01B)	Yueyang Aocheng Technology Co., Ltd (China)	<ul style="list-style-type: none"><li>• Maximum discharge voltage: 10,000 V</li><li>• Maximum emitting energy: 30 kJ</li><li>• Transmitting frequency: from <math>n \times 10</math> to <math>n \times 100</math> Hz</li></ul>
Three-component hydrophones (CDJ-JC100)	Chongqing Geological Instrument Factory (China)	<ul style="list-style-type: none"><li>• 12 electric vertical speed sensors in series</li><li>• Spacing: 1 m</li><li>• Central frequency: 100 Hz</li></ul>
RAS24 portable digital seismograph	ABEM (Sweden)	<ul style="list-style-type: none"><li>• Record length: 0.2 s</li><li>• Sample rate: 0.125 ms</li><li>• Pre-amp gain (PG): 12 db</li></ul>

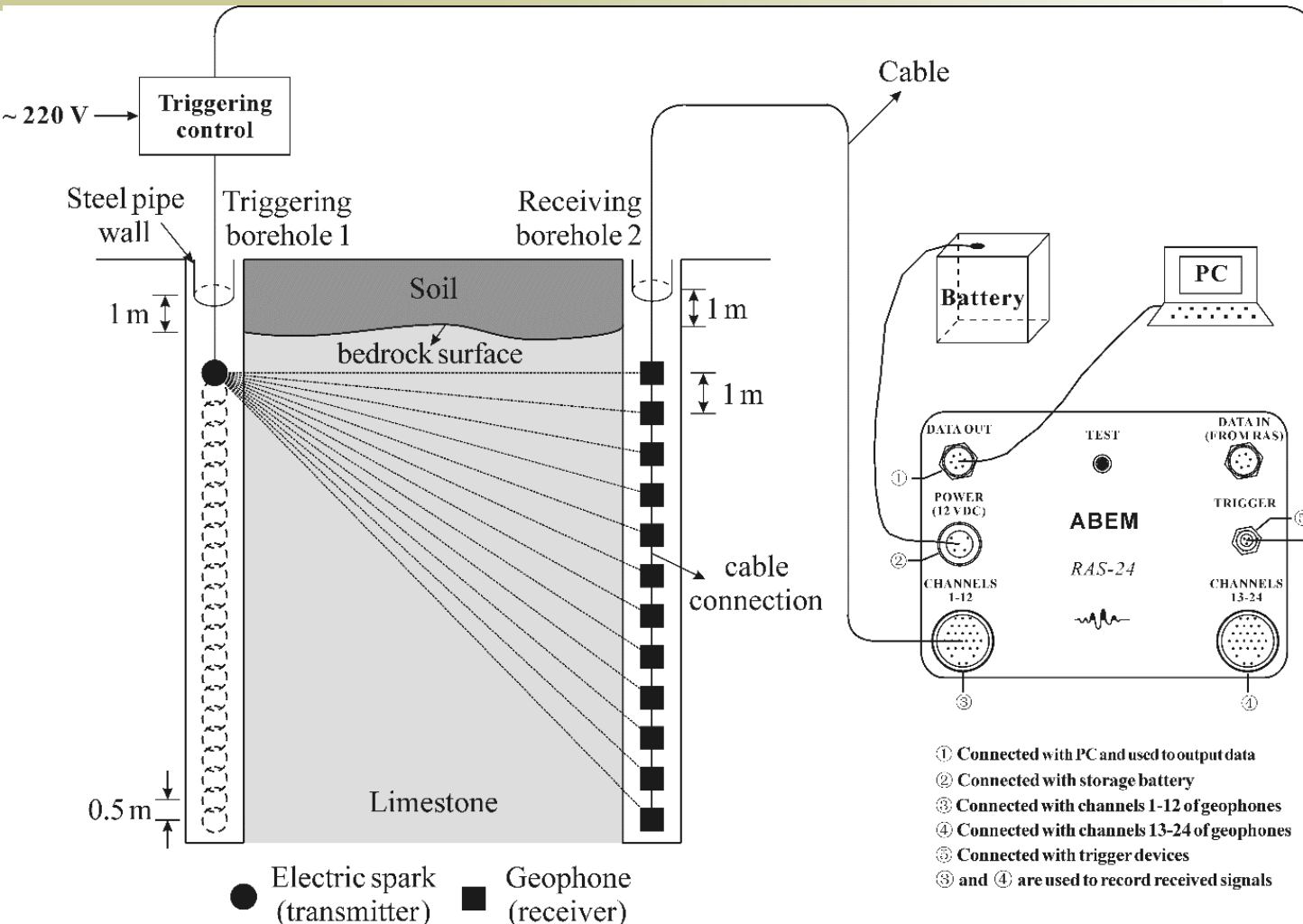




# Field data acquisition



## Test Procedures



Water table is below 30 m. So transmitter and geophones can be coupled through underground water.



# Seismic imaging (CT) technique



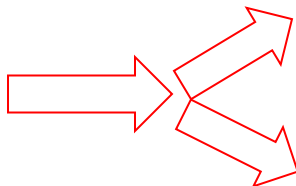
- Inversion of first arrival travel times

Wave energy traveling between a source and receiver is propagating along an infinitesimally narrow ray path.  $\Rightarrow$  General assumption

- Homogeneous model

$$t = \int_{x_s}^{x_r} s \cdot dl = Ls \Rightarrow L^T Ls = L^T t \Rightarrow \begin{cases} s = R^{-1} Q^T t \triangleq L^+ t \\ s = V S^{-1} U^T t \end{cases}$$

Low accuracy based on previous experiences



Flawed solving techniques ?

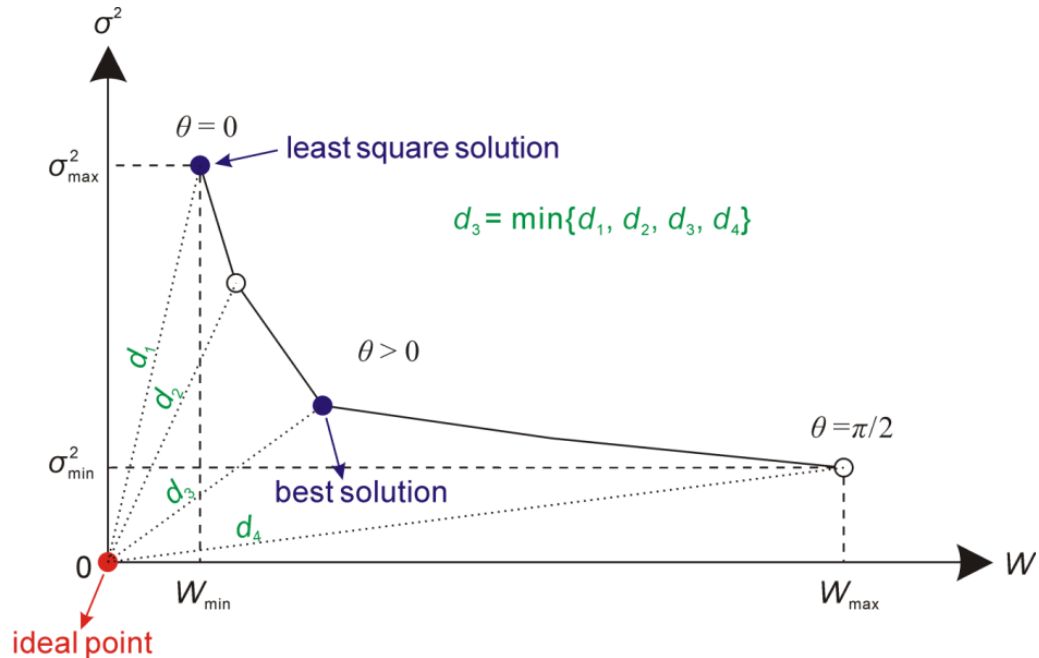
Improper model ?



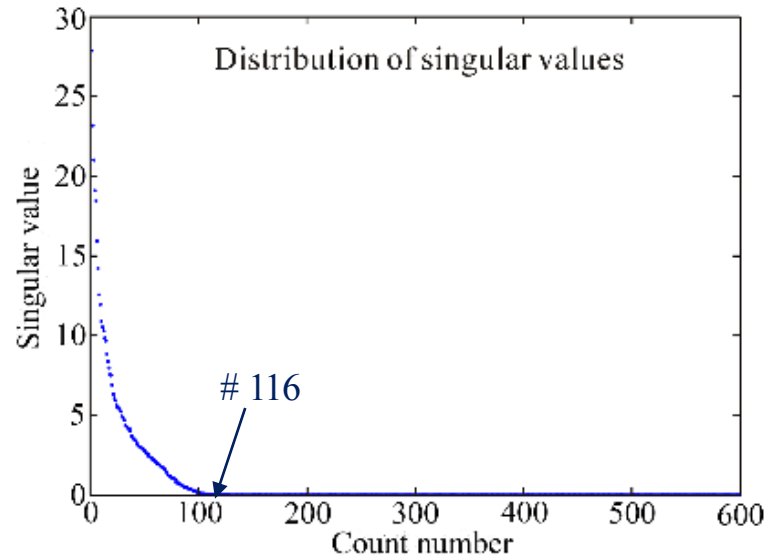
# Homogeneous model



A 600\*600 ill-posed matrix  
derived from a real case



After Backus and Gilbert (1970)



Resolution and stability  
are incompatible

Least square solution is not the best solution.



# Homogeneous model



- Ill-posed properties of  $L$
- Discard small singular values
- Unsatisfied resolution
- Remain large and revise small



Profiles	Residual norm $\  r \ _2$	Solution norm $\  s \ _2$
GW39-GW37	10.941983	20.896515
GW42-GW6	47.923083	17.971302

Although efforts were made to the algorithms,  
resolution and stability are far less than expected.

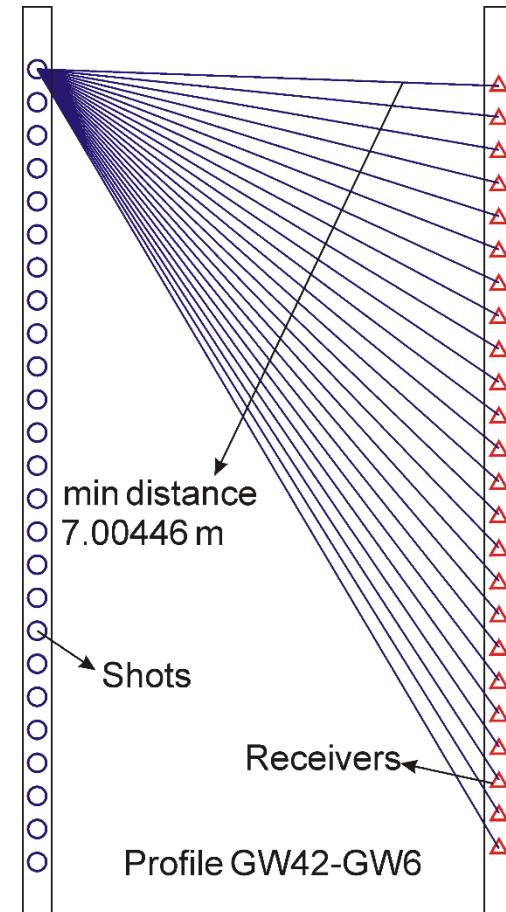


# It is the model that matters!



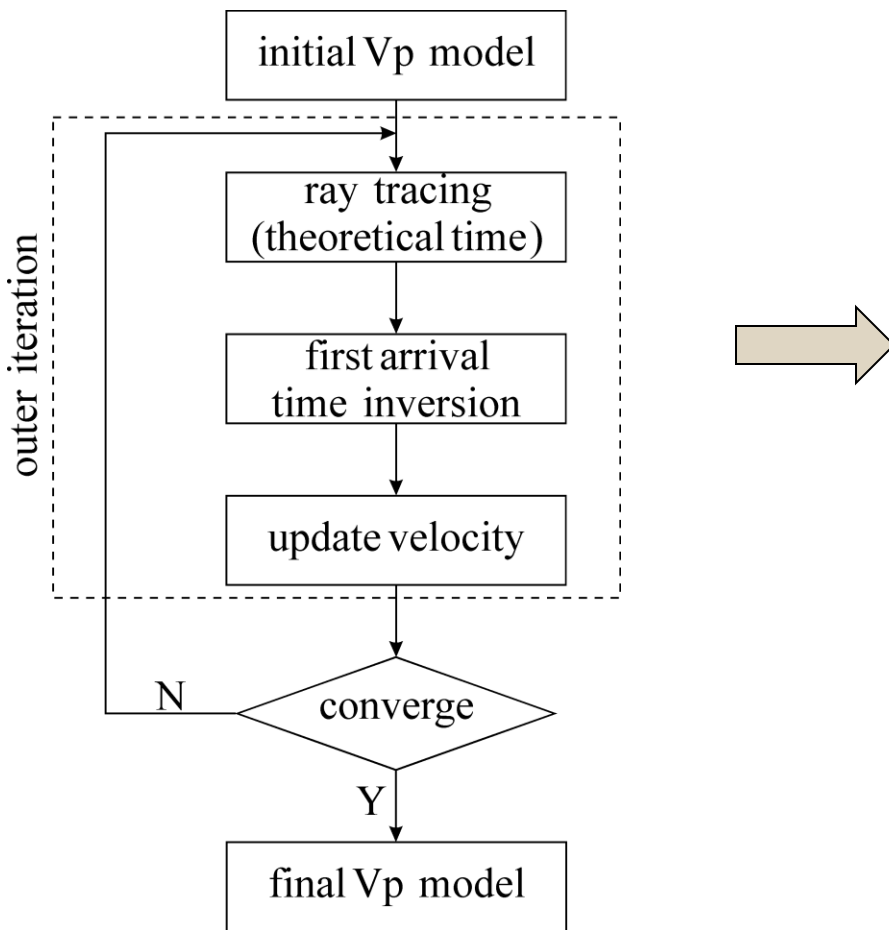
Direct rays can be used only when:

- **Velocity contrasts within 20%**
  - e.g.  $V_p$  for intact rock mass: 2.0 km/s
  - variance range: 1.6-2.4 km/s
  
- **Low-velocity anomalies are smaller than 15% the distance from source to receiver**
  - e.g. min distance: ~7 m
  - anomaly size: less than 1.05 m



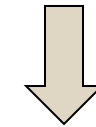


# Heterogeneous model



$$\mathbf{t} - \mathbf{t}^{(k+1)} = \mathbf{L}^{(k+1)} \Delta \mathbf{s}^{(k)}$$

$$\mathbf{s}^{(k+1)} = \mathbf{s}^{(k)} + \Delta \mathbf{s}^{(k)}$$



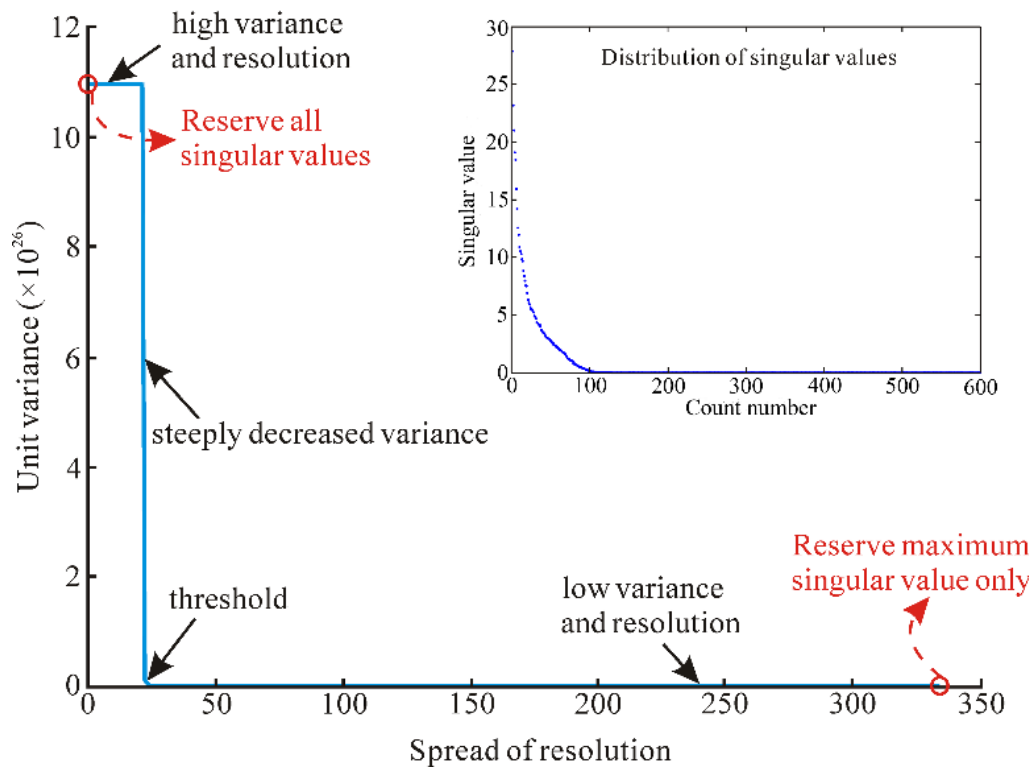
$\mathbf{s}^{(0)}$ ?

$\mathbf{L}^{(k)}$ ?

How to deal with the singularity of  $\mathbf{L}$ ?  
Inversion method?



# $s^{(0)}$ —initial P-wave velocity



Revision of singular values

$$\alpha'_k = \frac{\alpha_t^2}{\alpha_k} \quad k \geq q_t$$

$$\alpha'_k = \alpha_k + \frac{k}{q_t} \left( \frac{\alpha_t^2}{\alpha_{q_t+1}} - \alpha_{q_t} \right) \quad k < q_t$$

$$s_0 = VS_m^{-1}U^T t$$

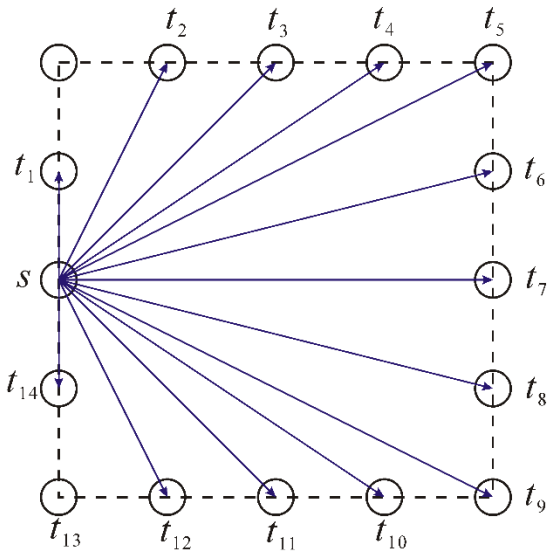
where  $S_m = \{\alpha'_k\}$



# $L^{(k)}$ – SPM ray tracing



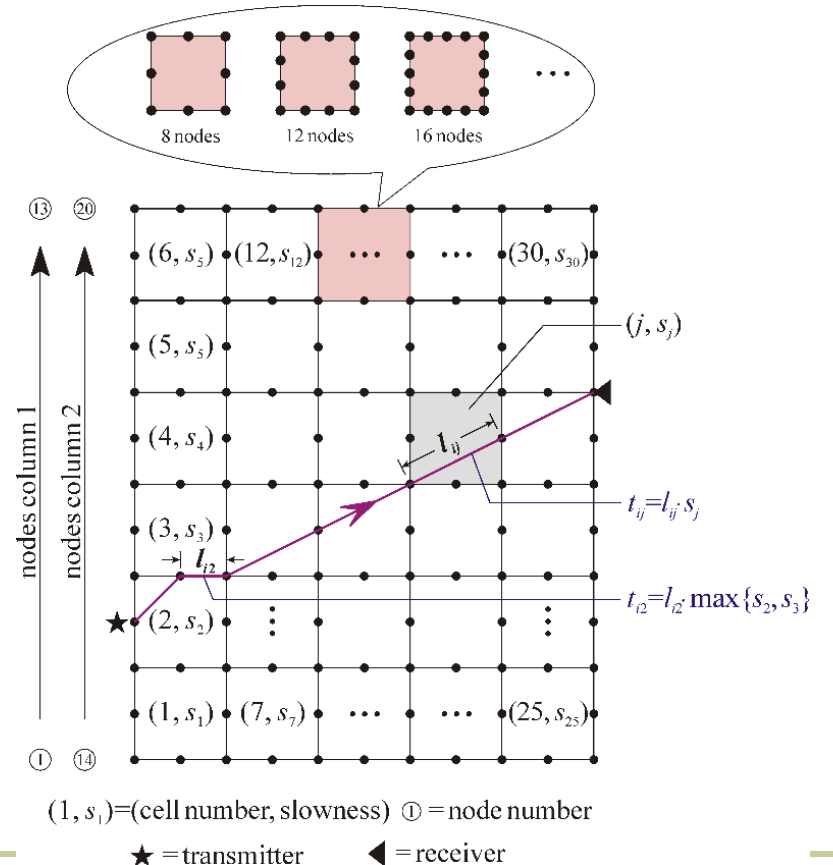
## ■ SPM = Shortest Path Method



○ node      → potential ray path  
s start       $t_n$  end

$$\{0, T_{s \rightarrow t_1}, T_{s \rightarrow t_2}, \dots, T_{s \rightarrow t_{12}}, T_{s \rightarrow t_{14}}\}$$

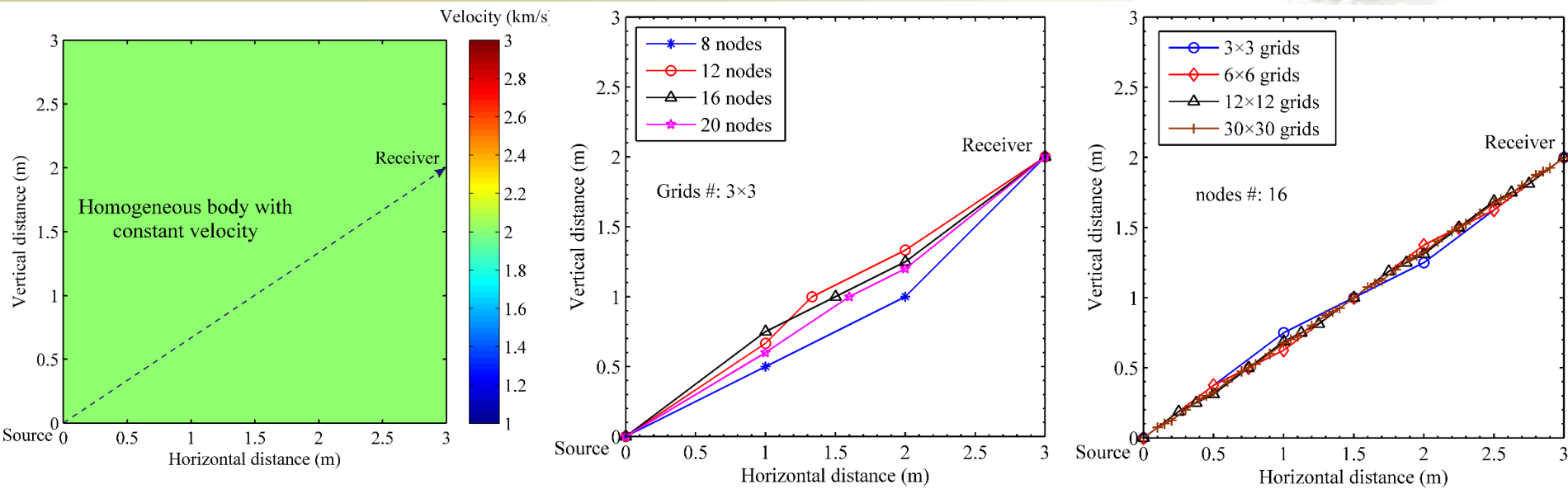
(e.g. Moser, 1991; Bai *et al.*, 2007;  
Cormen *et al.*, 2009)



Share the grid system with inversion



# $L^{(k)}$ – SPM ray tracing



16 nodes

Cell #	Node #	Th. 1st arr. time (ms)	Rel. err. (%)
$3 \times 3$	8	1.8251	1.24
	12	1.8106	0.43
	16	1.8095	0.37
	20	1.8071	0.24

Node #	Cell #	Th. 1st arr. time (ms)	Rel. err. (%)
16	$3 \times 3$	1.8095	0.37
	$6 \times 6$	1.8090	0.34
	$12 \times 12$	1.8090	0.34
	$30 \times 30$	1.8090	0.34



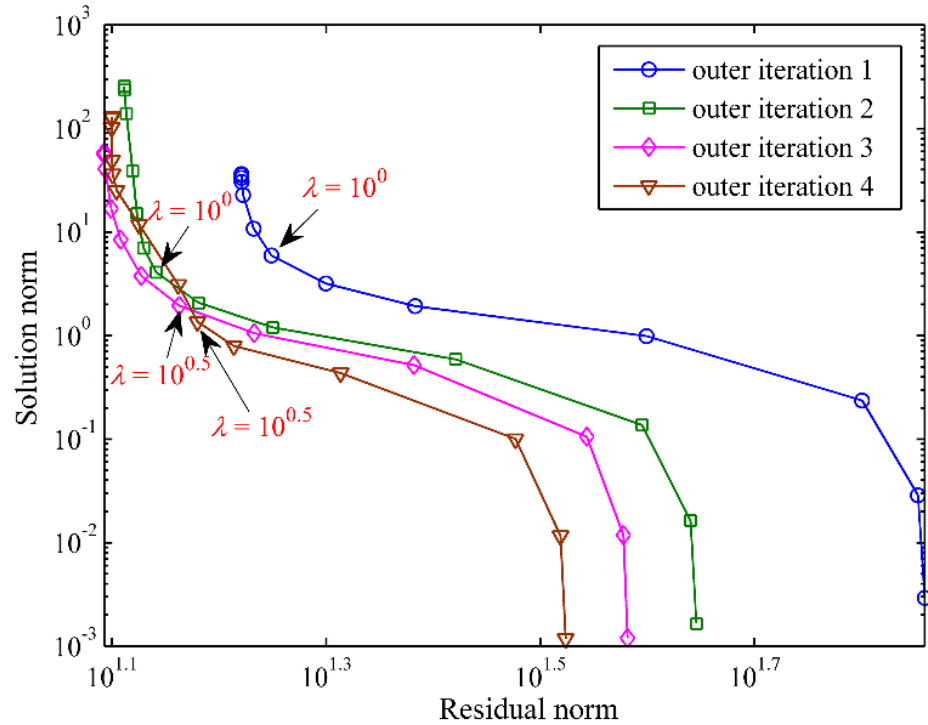
# Singularity of $L$ -regularization



$$\mathbf{t}_{m \times 1} = \mathbf{L}_{m \times n} \mathbf{s}_{n \times 1} \iff \min \left\| \begin{bmatrix} \mathbf{L} \\ \lambda \mathbf{I} \end{bmatrix} \mathbf{s} - \begin{bmatrix} \mathbf{t} \\ 0 \end{bmatrix} \right\|_2 \quad (\text{Aster et al., 2013})$$

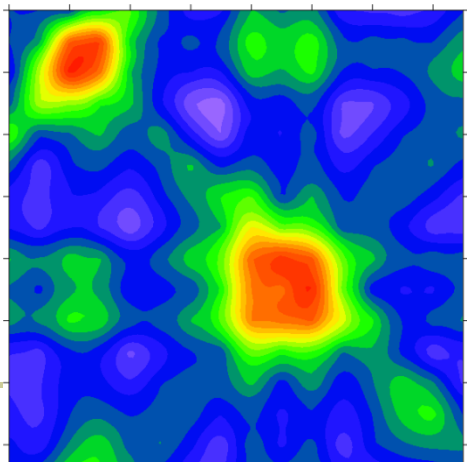
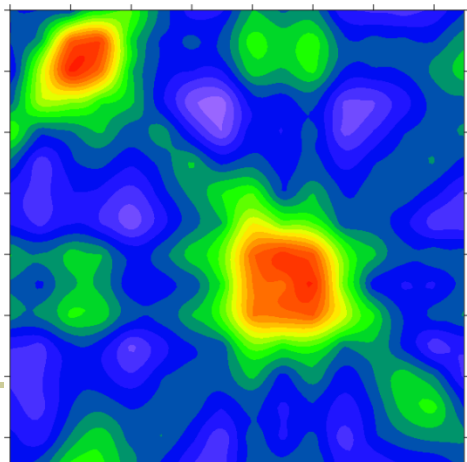
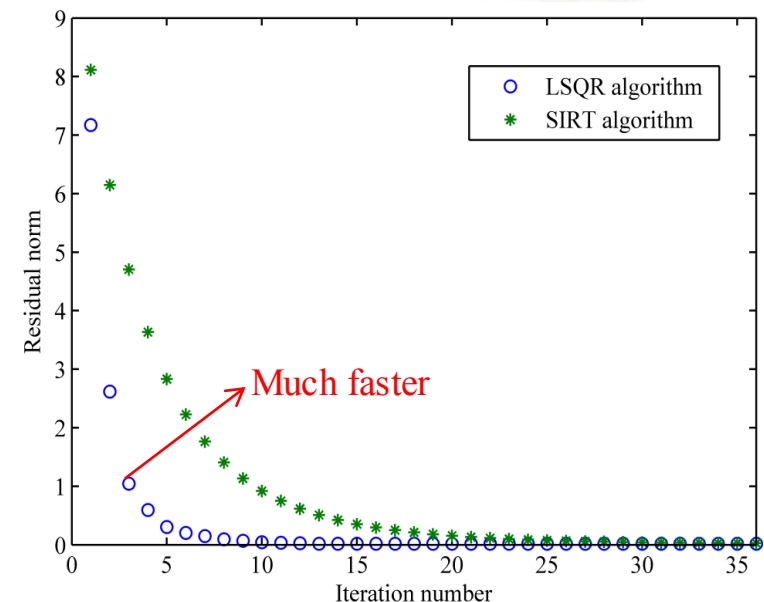
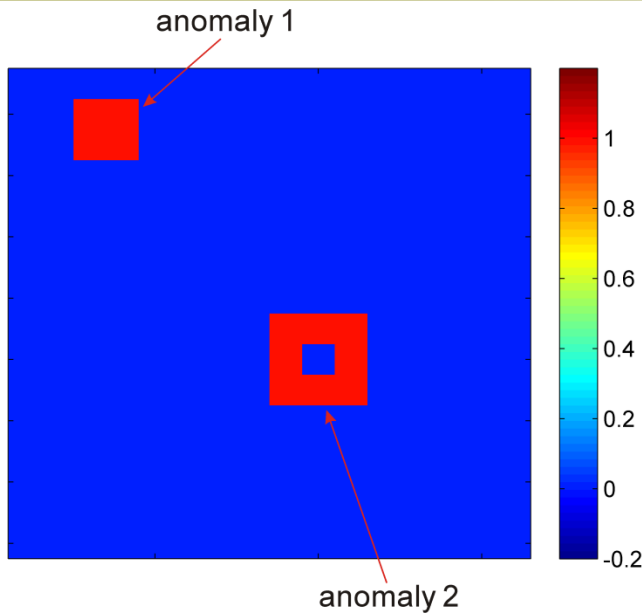
$$\begin{bmatrix} \mathbf{L} \\ \lambda \mathbf{I} \end{bmatrix} \mathbf{s} = \begin{bmatrix} \mathbf{t} \\ 0 \end{bmatrix}$$

- $\|\mathbf{L}\mathbf{s}-\mathbf{t}\|_2$  vs  $\|\mathbf{s}\|_2$  curves
- The optimal damping factor ( $\lambda$ ), among  $10^{-5}, 10^{-4.5}, 10^{-4}, \dots, 10^{2.5}, 10^3$
- The best compromised solutions





# Inversion method—LSQR



---

Inv. algm.	Rel. err.	Iter. #	CPU time (s)
SIRT	0.654	200	0.0938
LSQR		36	0.0045



# Summary



Nonlinear problem

$$\mathbf{t} - \mathbf{t}^{(k+1)} = \mathbf{L}^{(k+1)} \Delta \mathbf{s}^{(k)}$$

$$\mathbf{s}^{(k+1)} = \mathbf{s}^{(k)} + \Delta \mathbf{s}^{(k)}$$

Inverse the P-wave  
velocity of each cell

Linearize

$$\Delta \mathbf{t}_i^{(k)} = \sum_{j=1}^N \mathbf{L}_{ij}^{(k+1)} \Delta \mathbf{s}_j^{(k)}$$

$$\Delta \mathbf{t}_i^{(k)} = |\mathbf{t}_{\text{obs}} - \mathbf{t}^{(k+1)}|$$

$$\mathbf{s}_j^{(k+1)} = \mathbf{s}_j^{(k)} + \Delta \mathbf{s}_j^{(k)}$$

Regularize

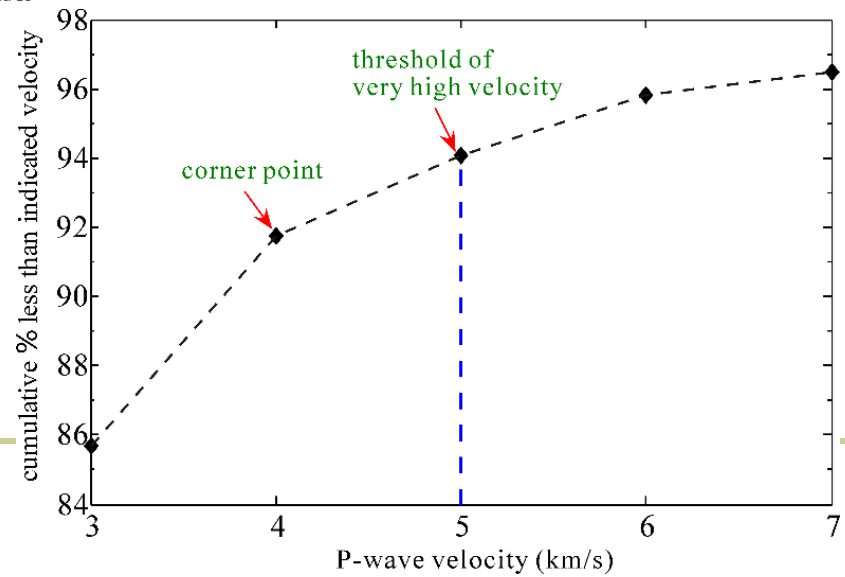
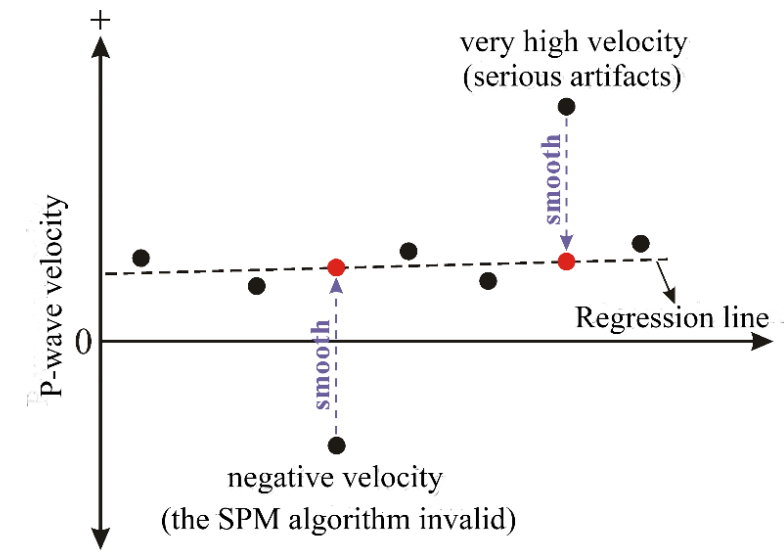
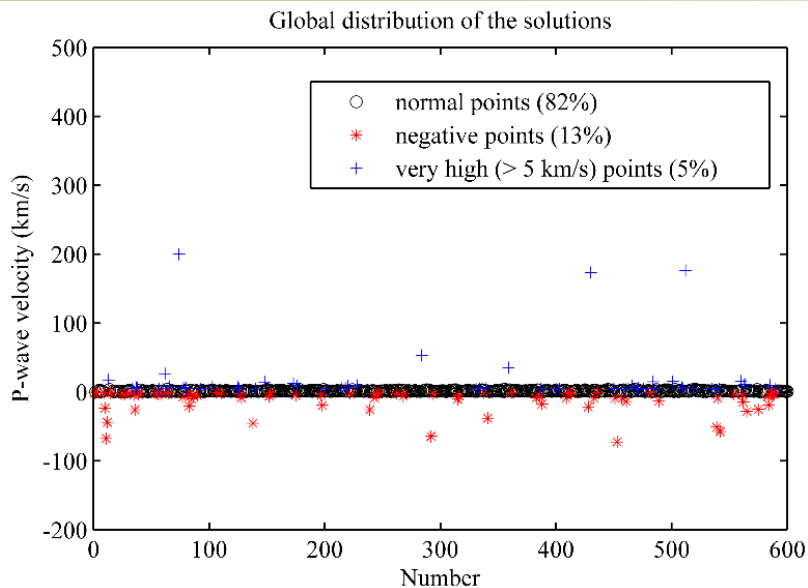
$$\min \left\| \begin{bmatrix} \Delta \mathbf{t} \\ 0 \end{bmatrix} - \begin{bmatrix} \mathbf{L} \\ \lambda \mathbf{I} \end{bmatrix} \Delta \mathbf{s} \right\|_2$$

$$\Delta \mathbf{s}^{(0)} = 0$$

Iterate using LSQR

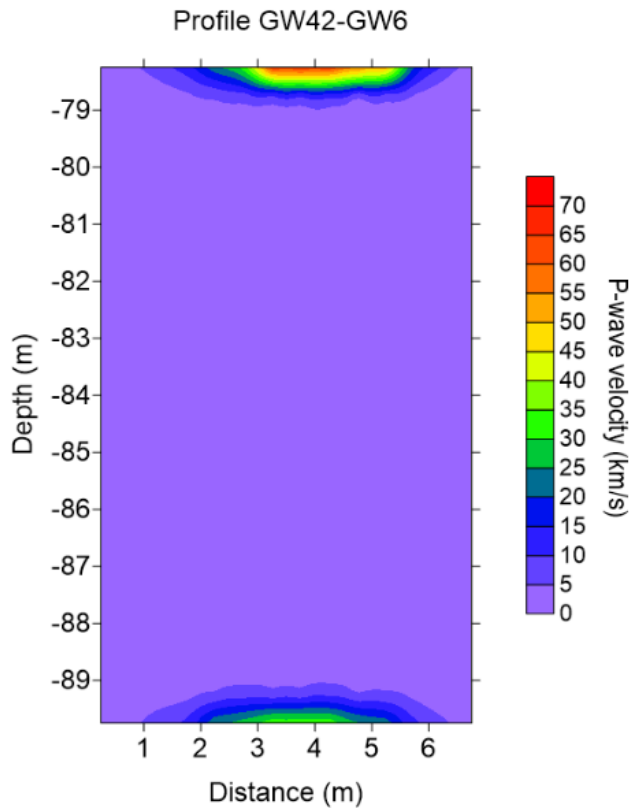


# Velocity corrections

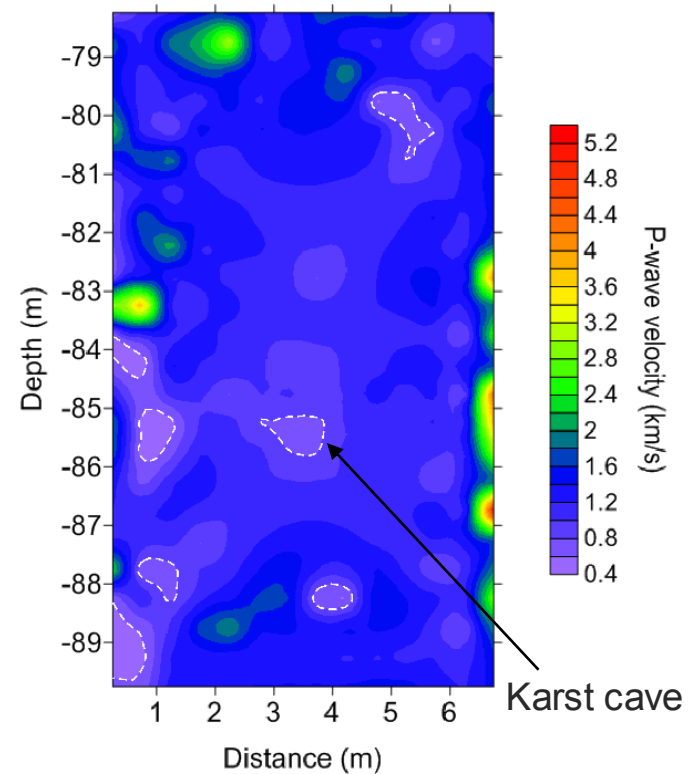




# Velocity corrections



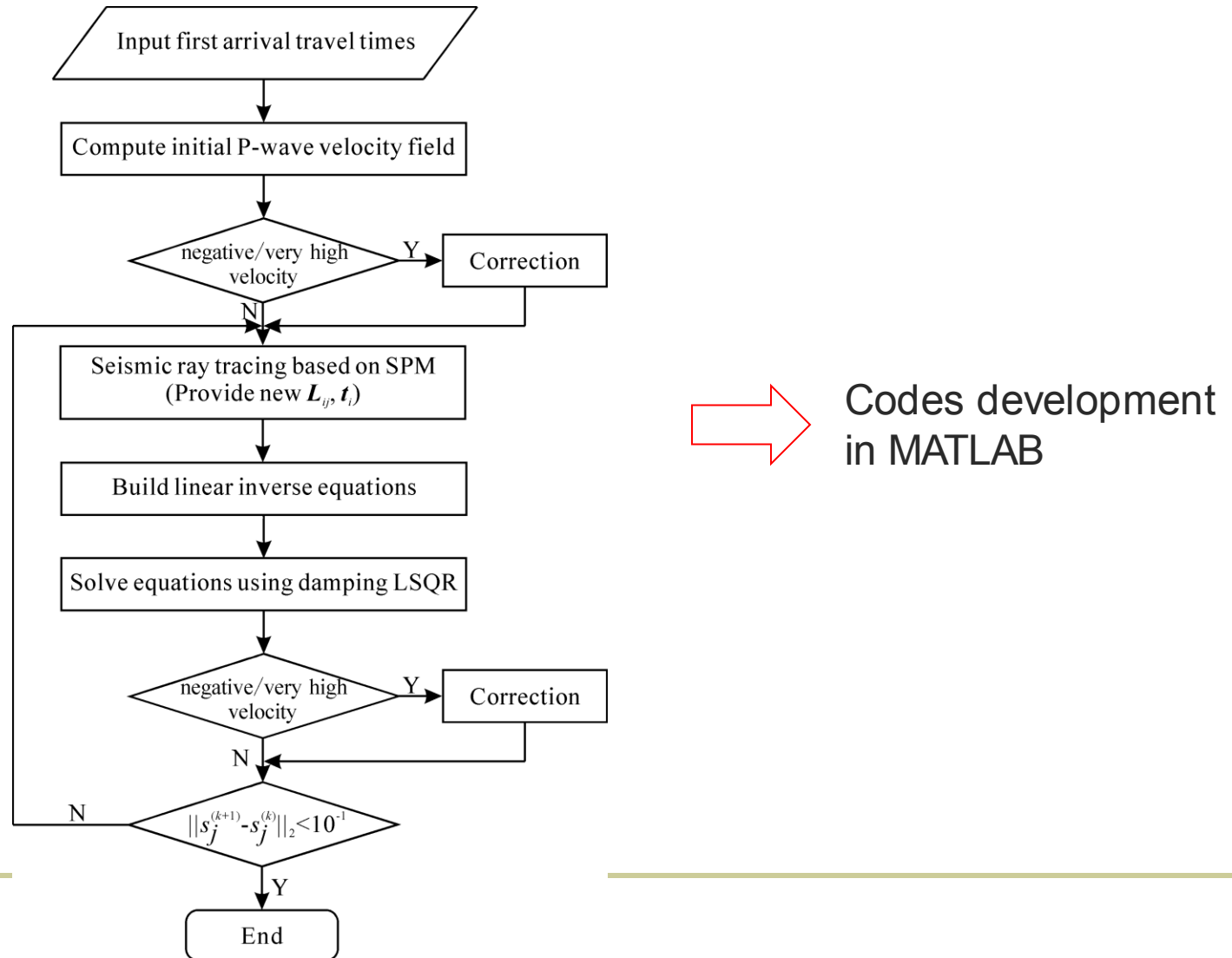
Before correction



After correction

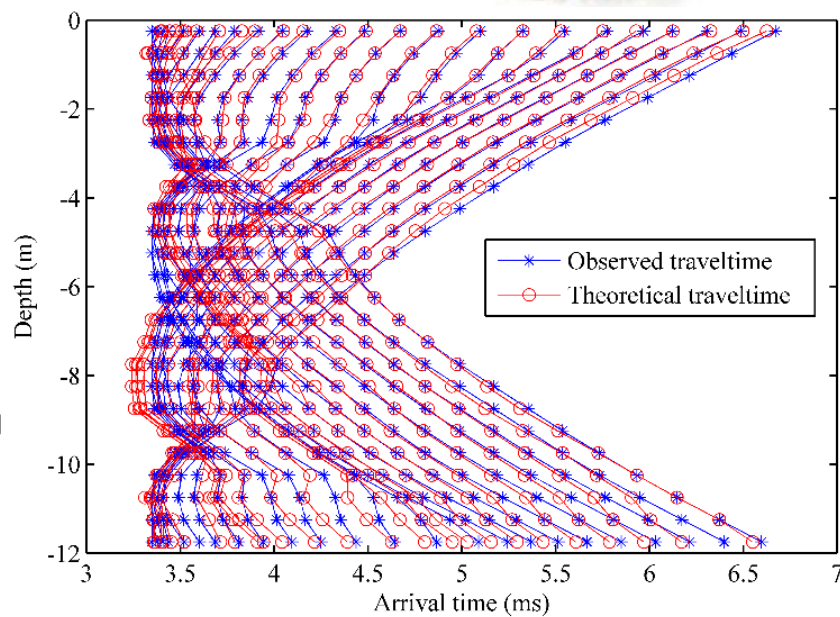
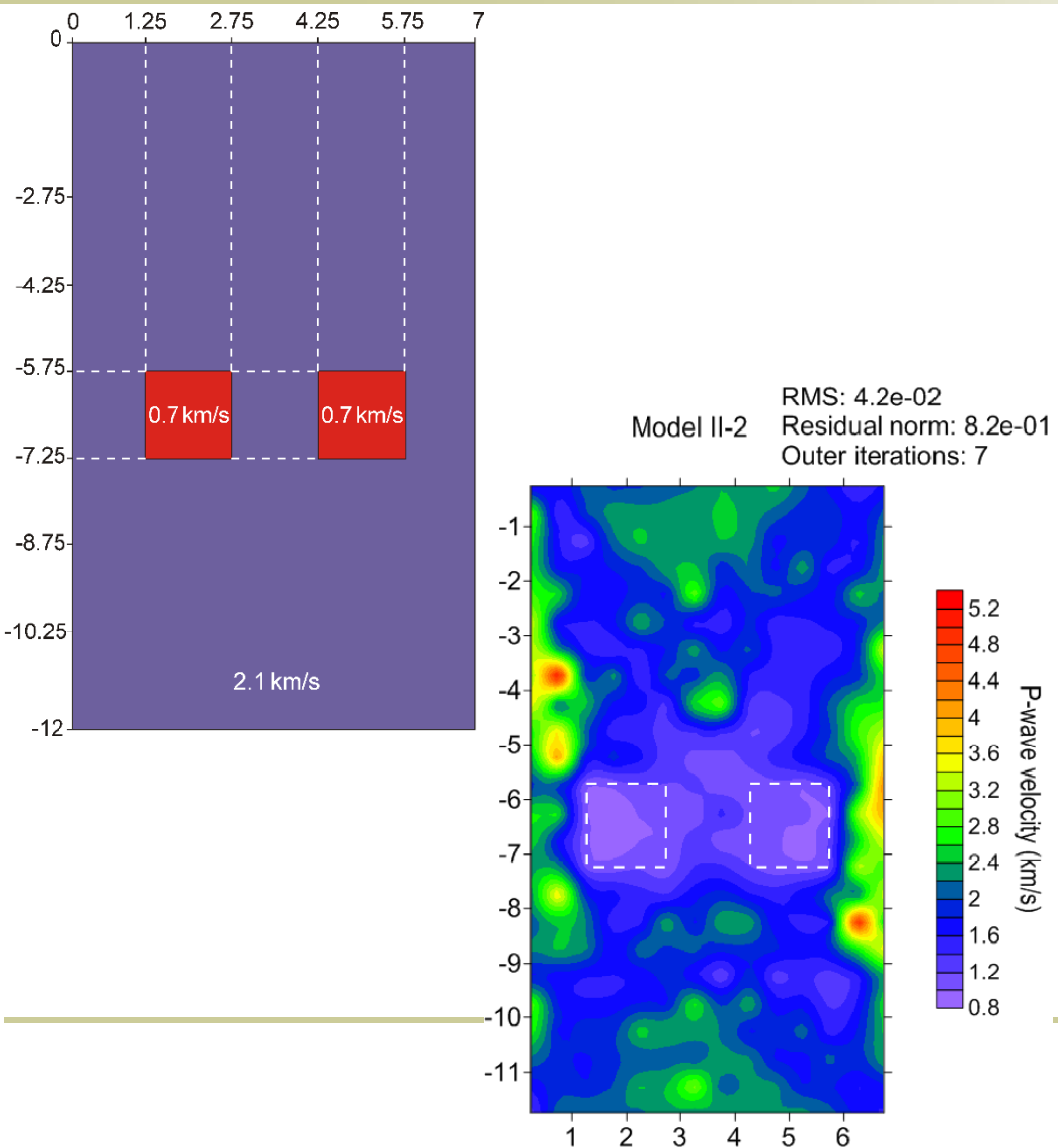


# Complete computing process



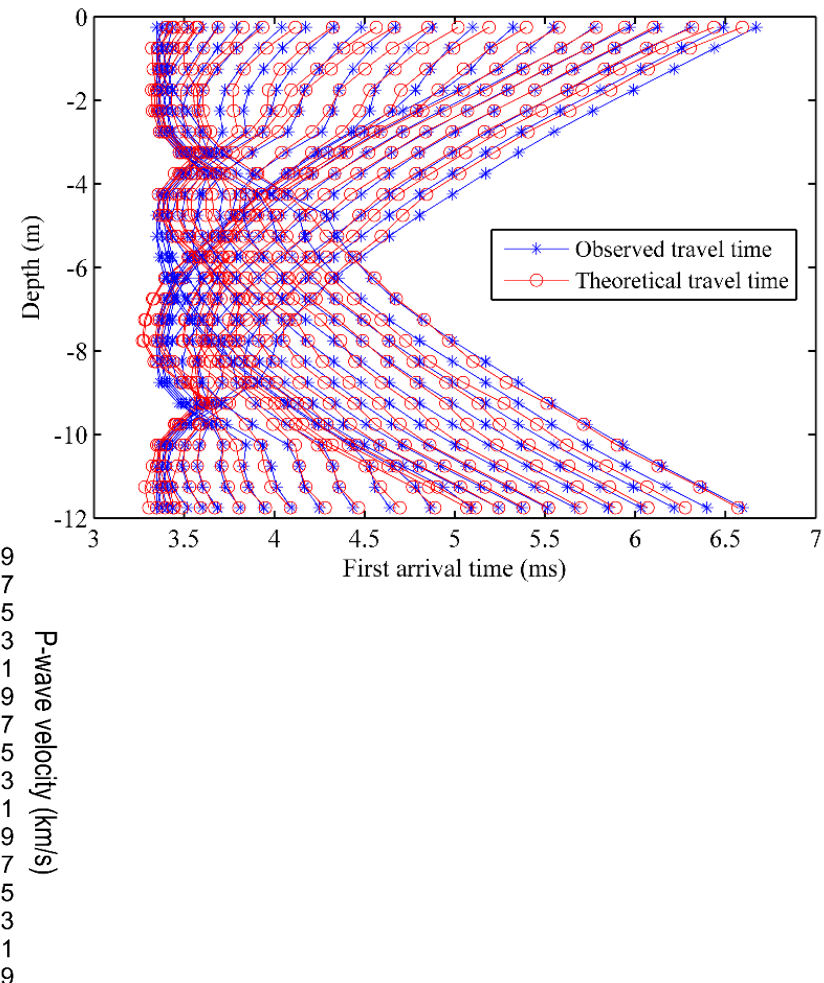
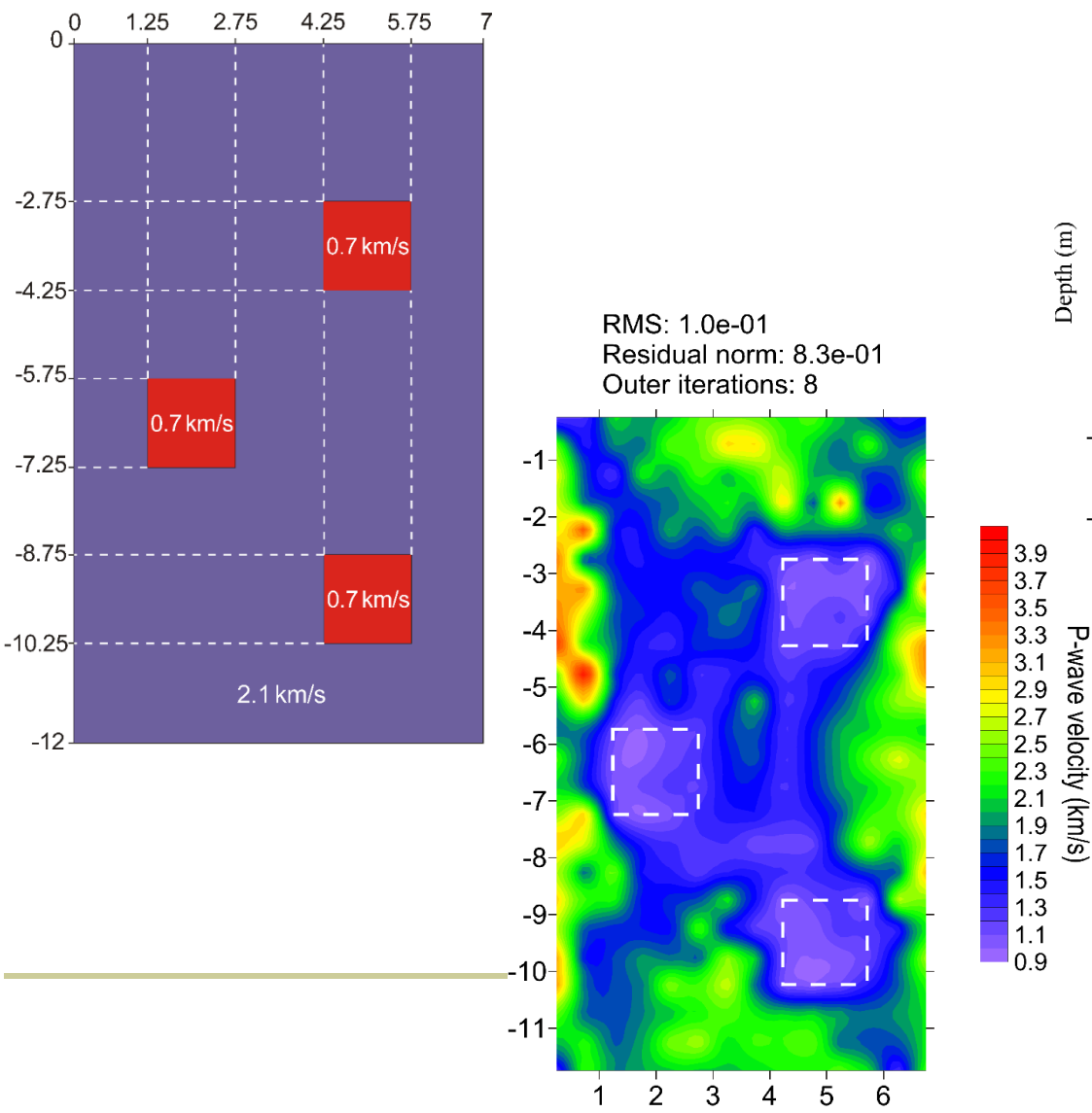


# Synthetic models





# Synthetic models





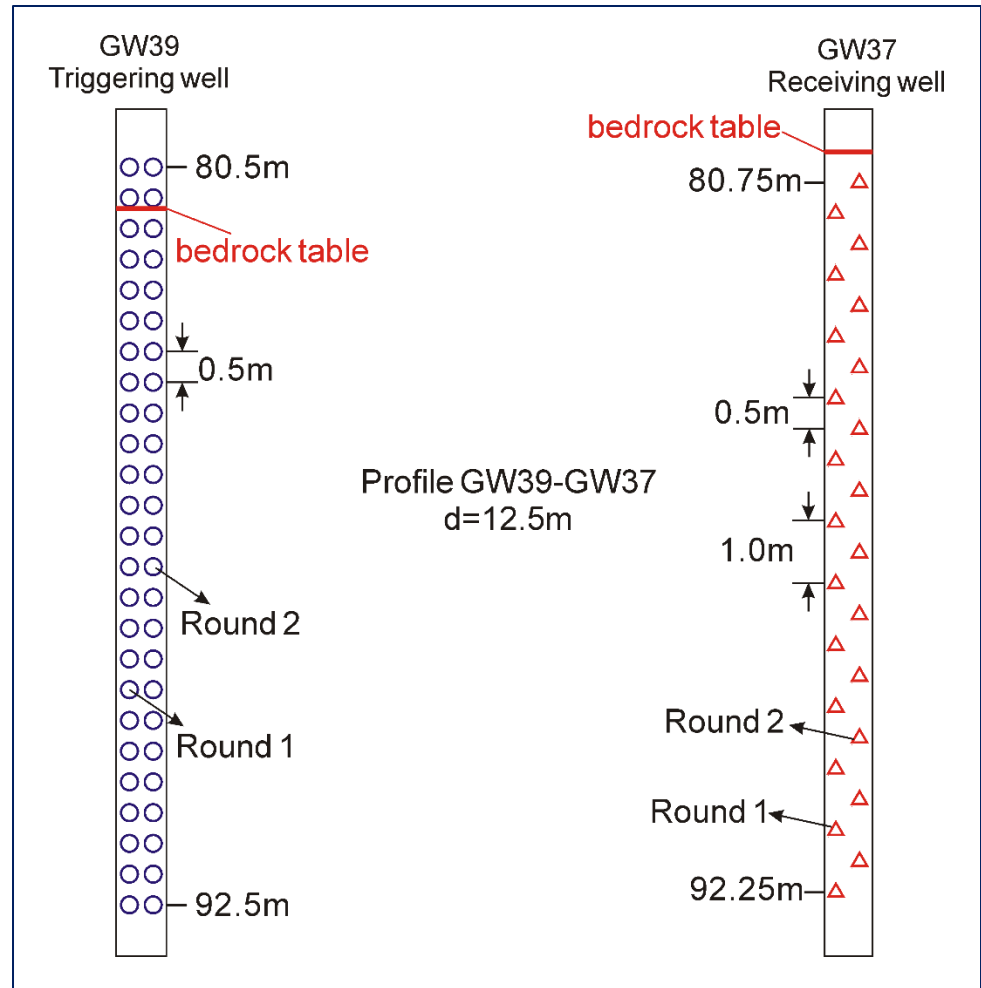
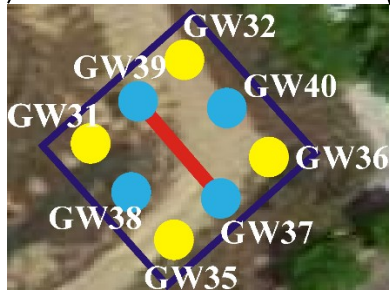
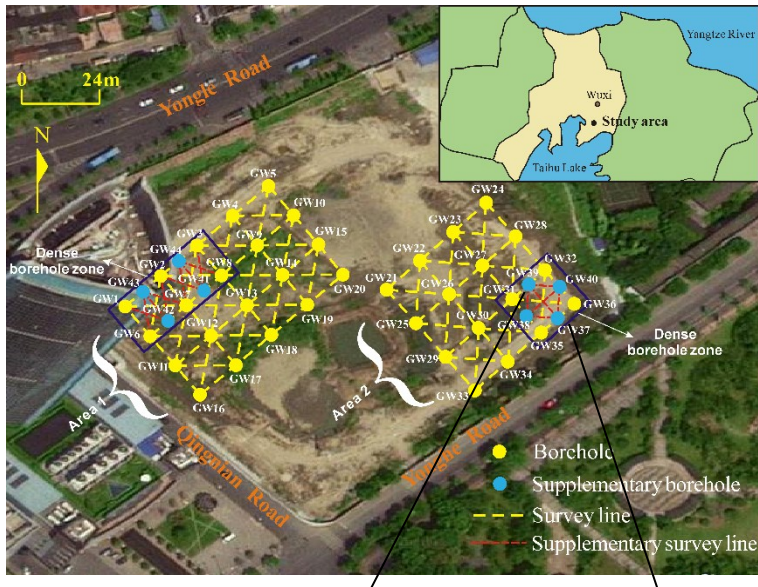
# Synthetic models



- For residual norm and RMS, the orders of magnitude are all below  $10^{-1}$ .
- Velocity disparities are obvious between anomalies and surrounding rock mass.
- Positions of anomalies are close to those in the true model.
- Sporadic anomalies are inevitably occurred for travel time inversion. They have to be verified by drilling data.
- The inverted velocities of the anomalies are somewhat high ( $\sim 0.8\text{-}0.9 \text{ km/s}$ ). But the relative errors are in an acceptable range.

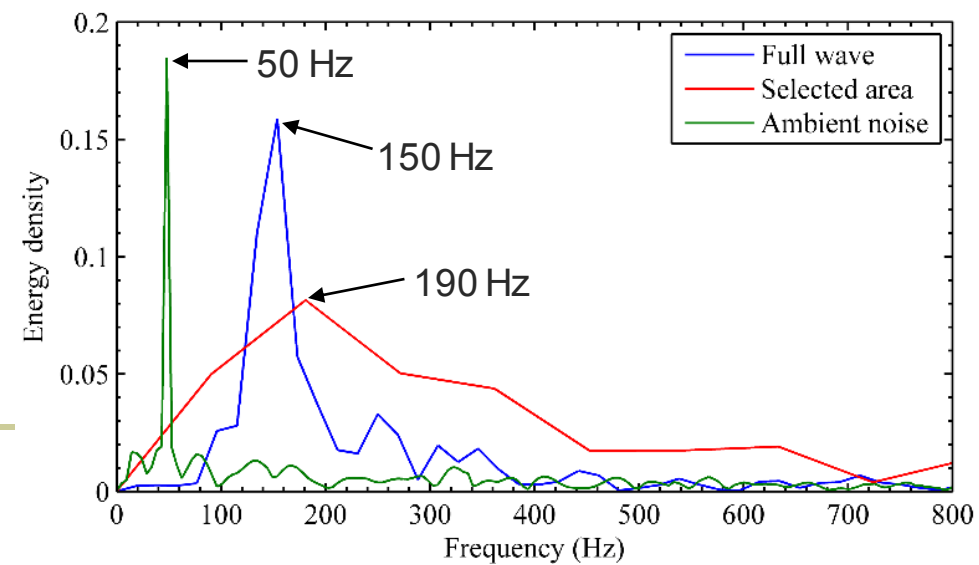
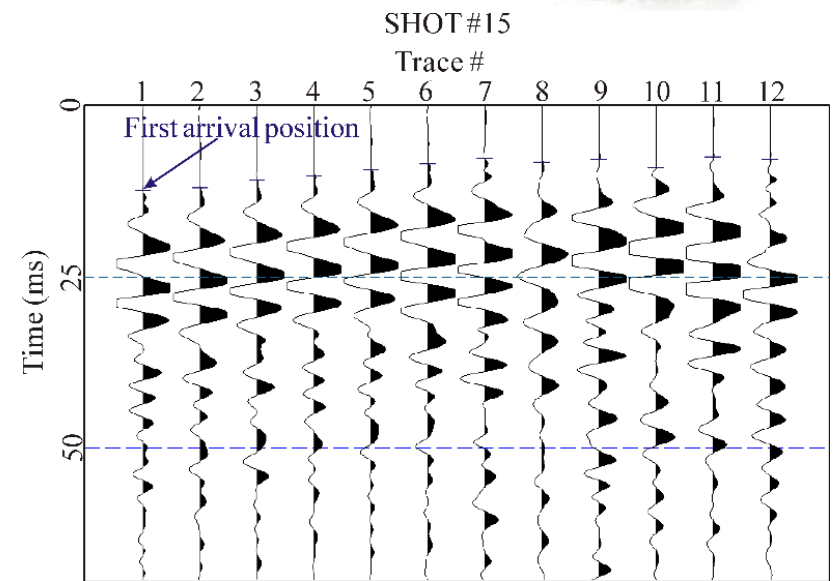
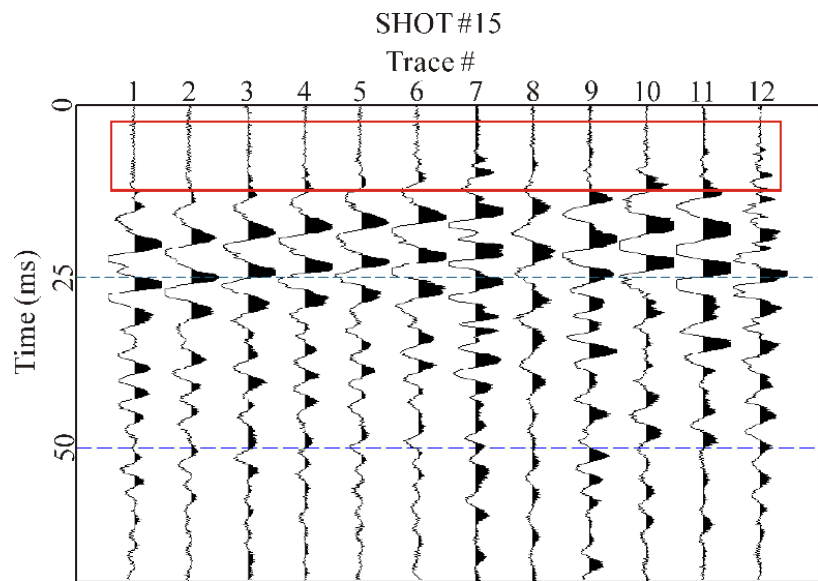


# Results and interpretations





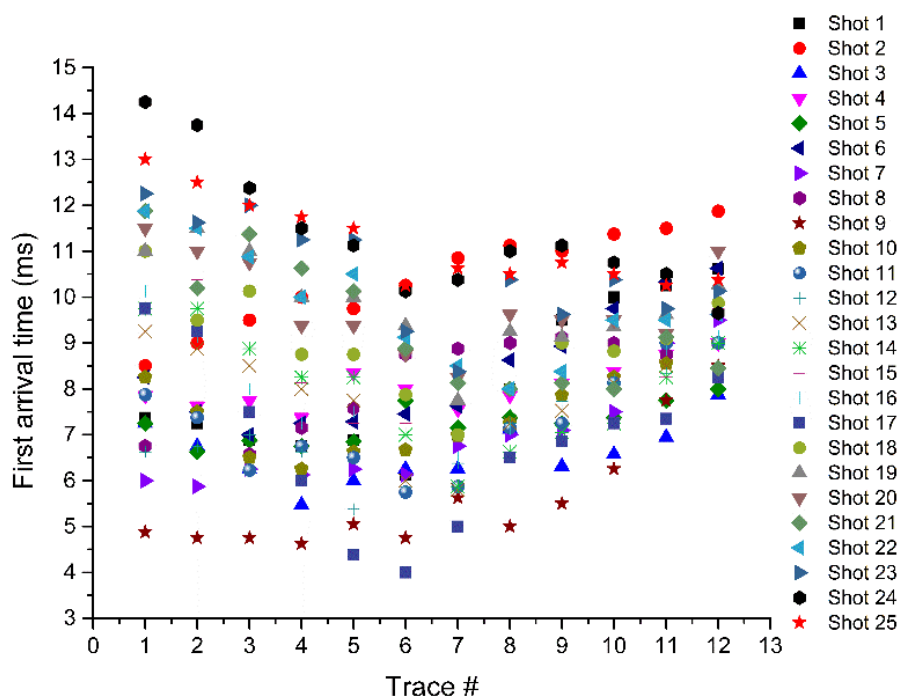
# Waveform analysis



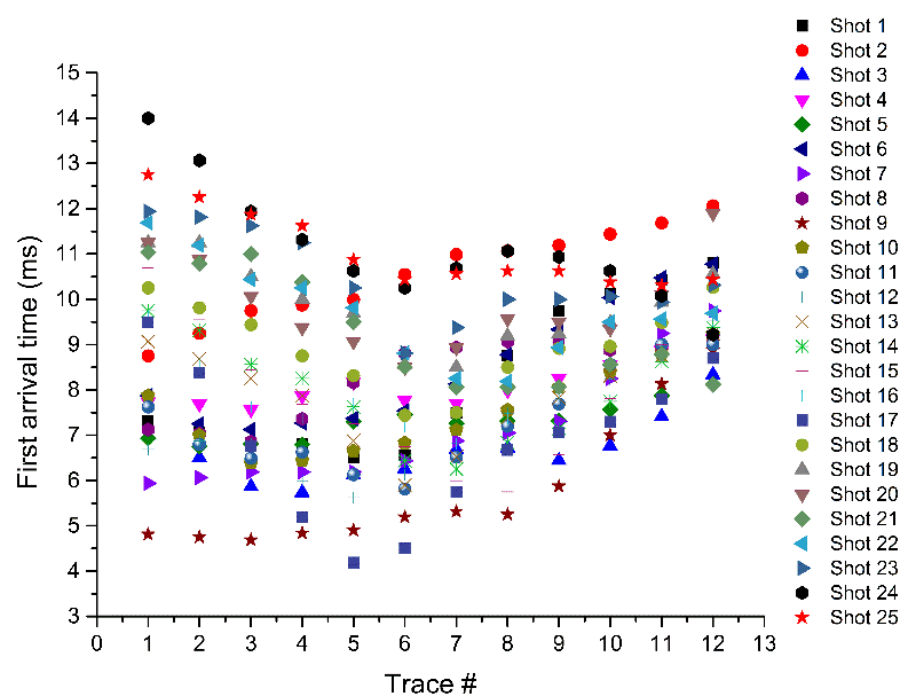
Bandpass filter:  
L: 70 Hz / H: 250 Hz



# Waveform analysis



First arrival travel times (Round 1)



First arrival travel times (Round 2)



# Cell dimension



- Discernable scale: (1/8~1/4) wavelength (Fowler, 1990)

$$(1/8, 1/4]\text{wavelength} = (1/8, 1/4] \times \frac{0.5 \text{ km/s}}{190 \text{ Hz}} = (0.33, 0.66] \text{ m}$$

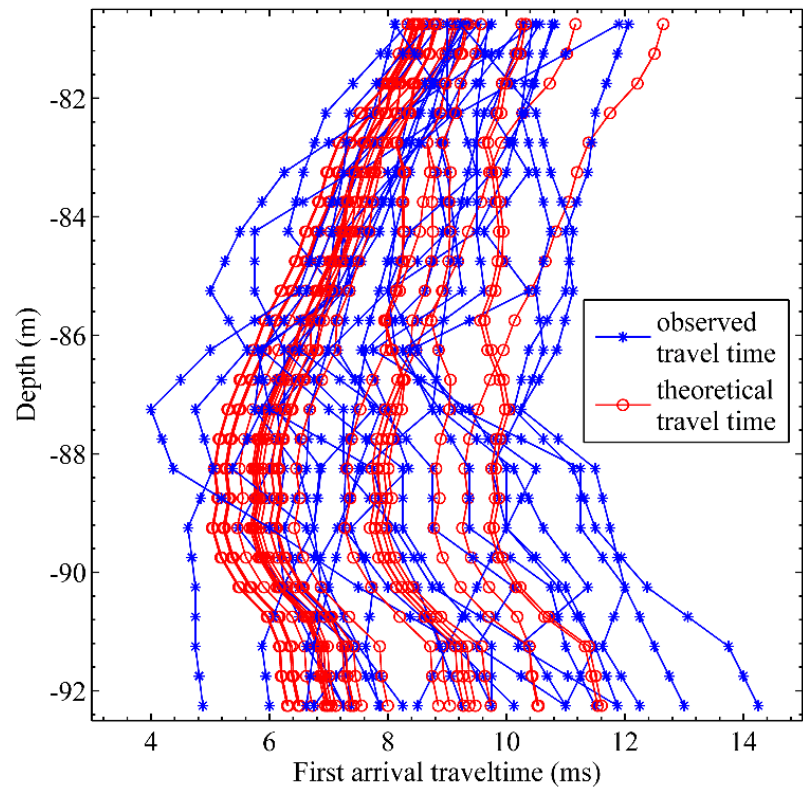
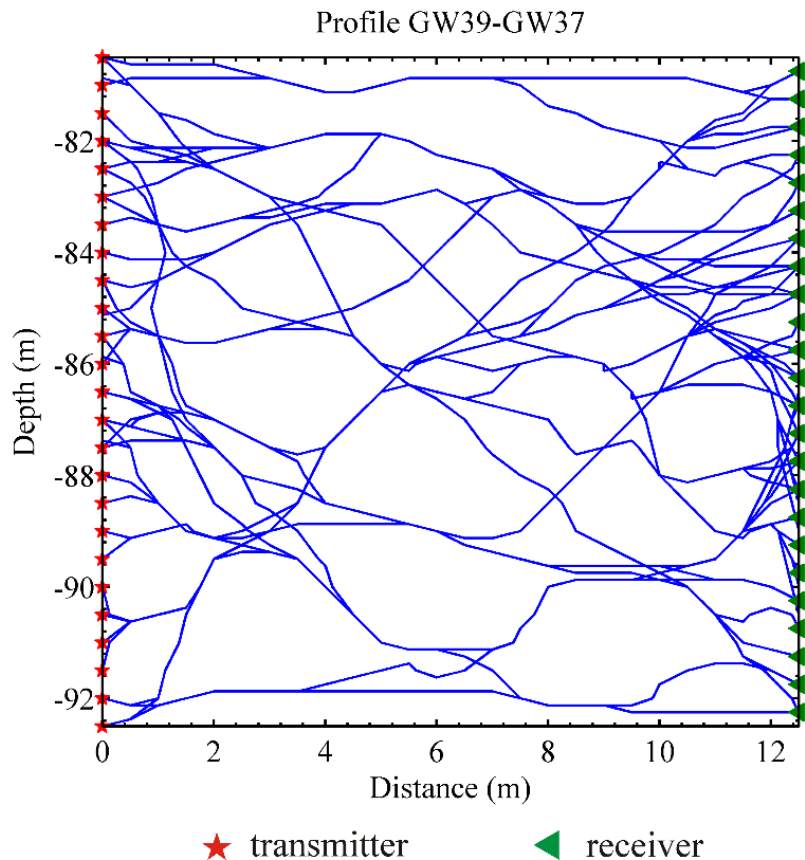
- Not exceed 1/3 the scale of the detecting target  
(Dziewonski and Woodhouse, 1987)

$$\text{cell dimension} < 1/3 \times \text{aver. diameter} = 1/3 \times 1.58 \text{ m} = 0.53 \text{ m}$$

- To be consistent with the acquisition geometry, cell dimension = 0.5 m
- 600 cells, 4,397 nodes (16 nodes per cell)

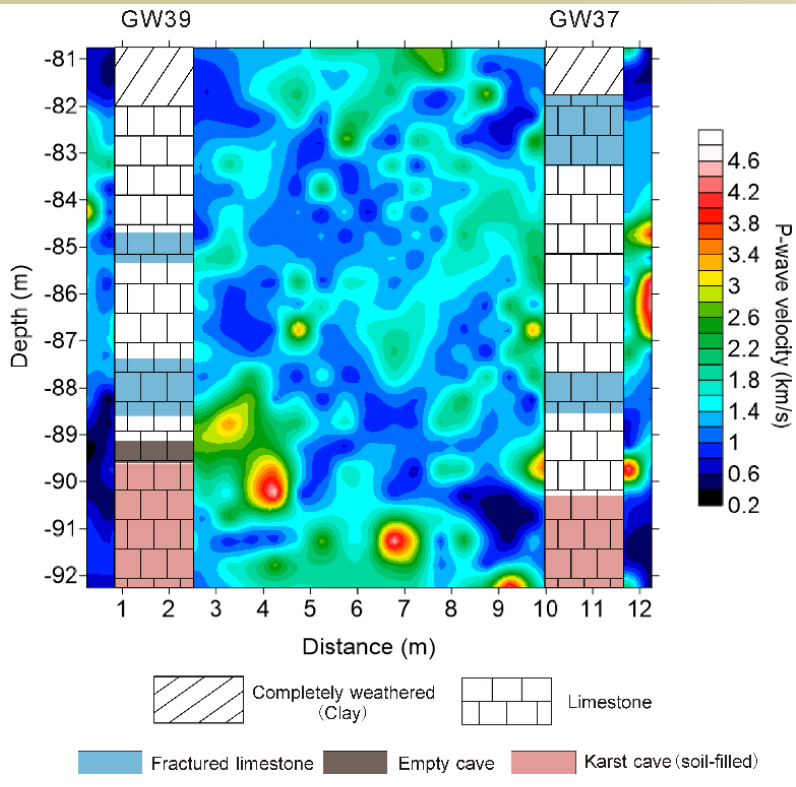


# Results I





# Results II – interpretation criteria



Category of detected anomalies	P-wave velocity (km/s)
Karst cave with void	< 0.4 ( $\pm$ 0.1) <sup>a</sup>
Karst cave with cohesive soil fill (or completely weathered layer)	0.4 to 1.0 ( $\pm$ 0.1) <sup>a</sup>
Fractured limestone	1.0 to 1.4 ( $\pm$ 0.1) <sup>a</sup>

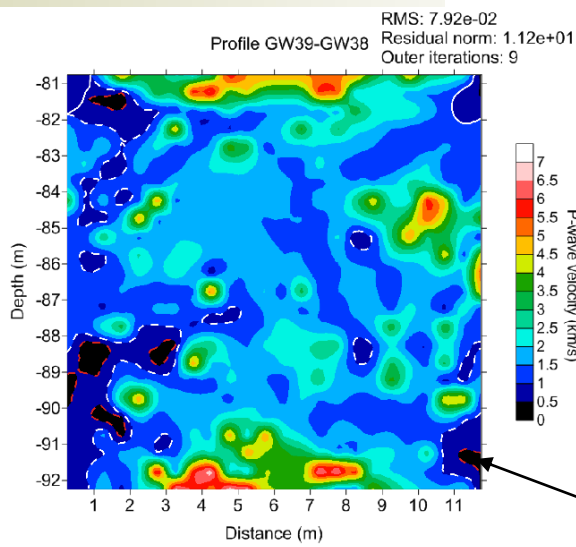
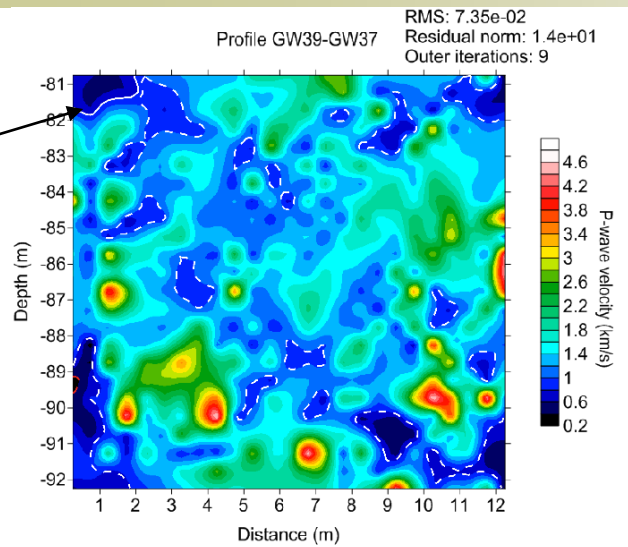
<sup>a</sup> The minimum interval of velocity contours is 0.2 km/s, so 0.1 km/s is the maximum error of the tomographic image.



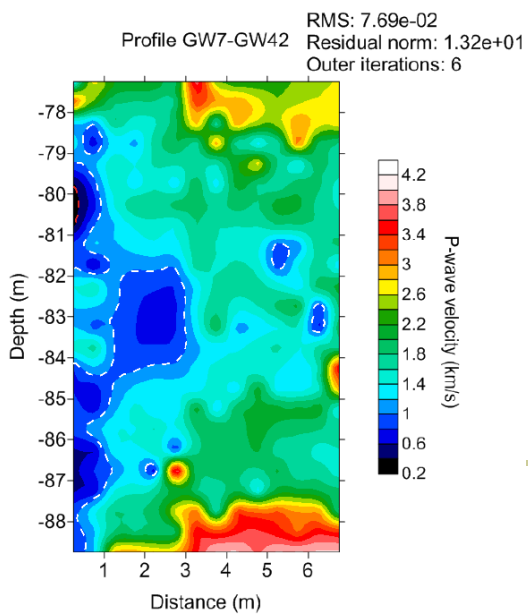
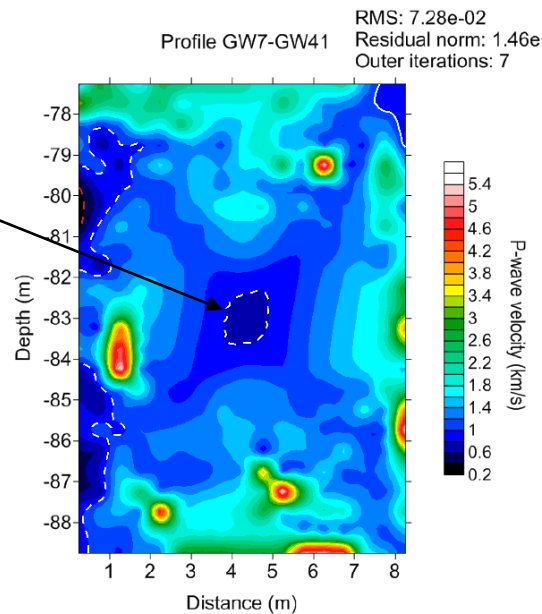
# Results III



Completely weathered layers (clay)

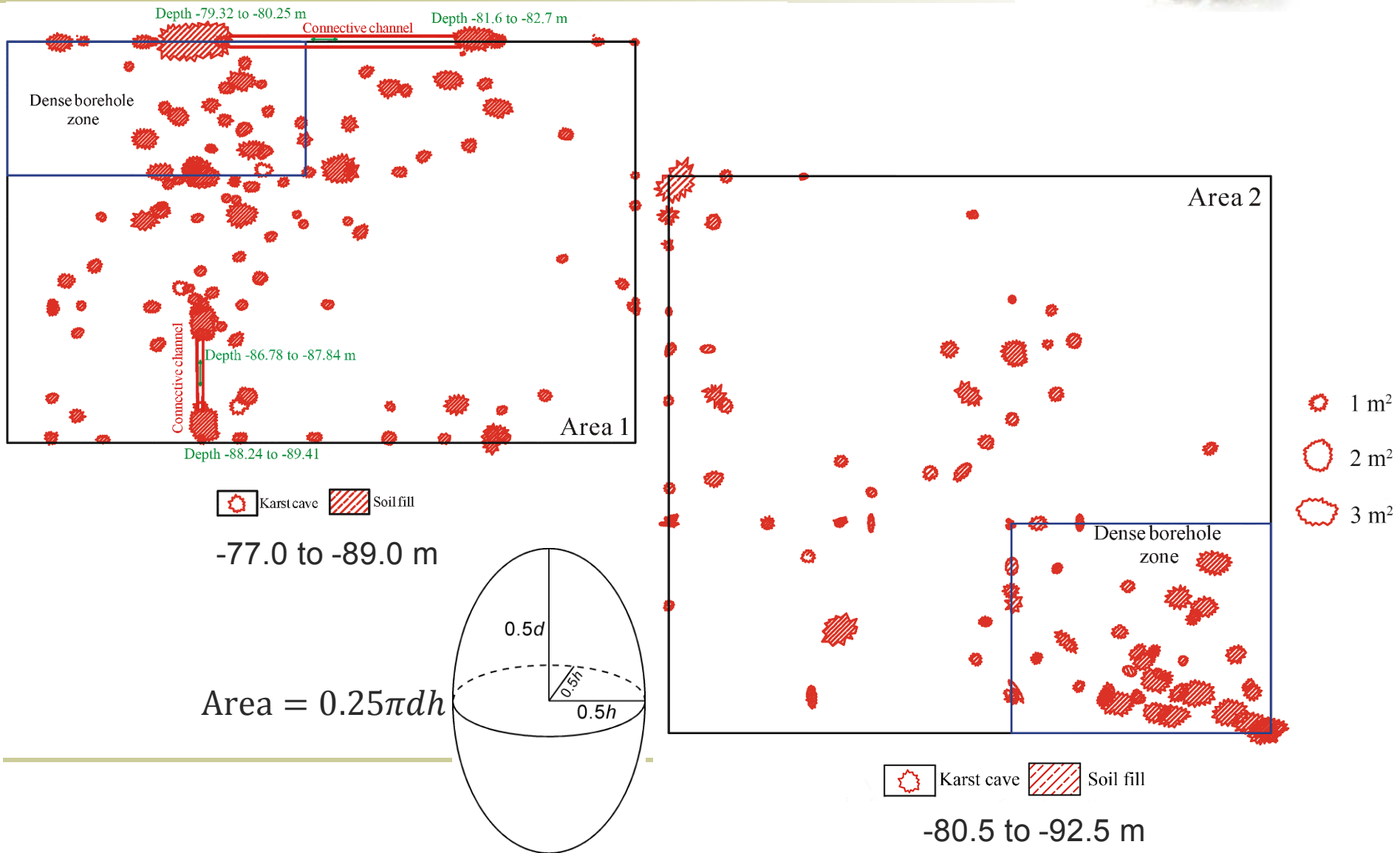


Cohesive soil fill





# Planar distribution of karst caves





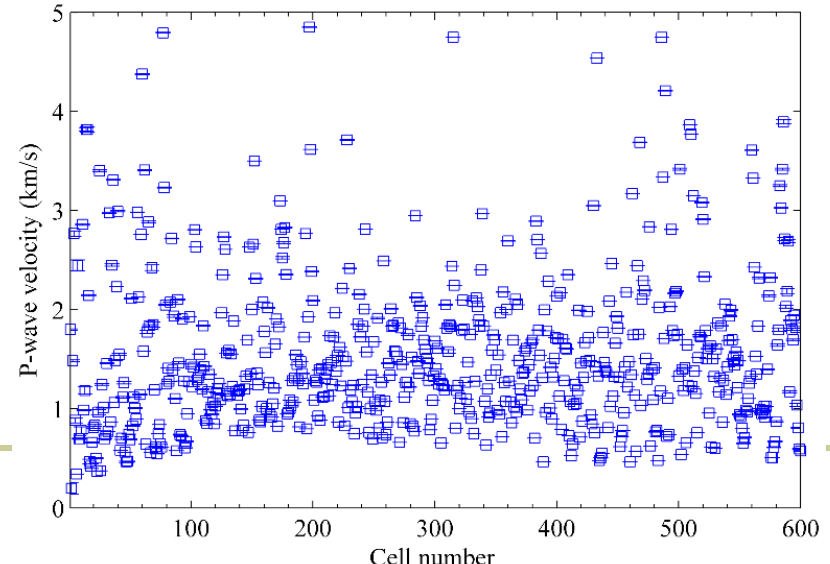
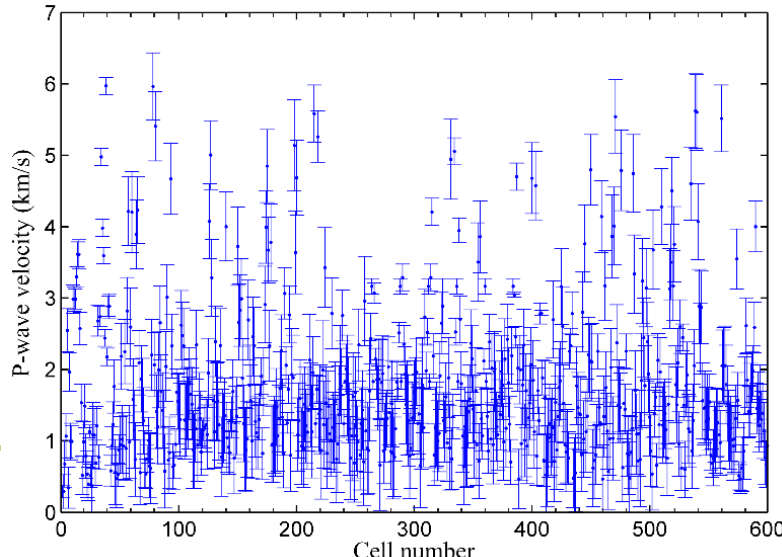
# Reliability analysis



resolution

stability

Inverted profile	Residual norm $\ r\ _2$		Rate of change (%)	Solution norm $\ s\ _2$		Rate of change
	Initial	Final		Initial	Final	
GW39-GW37	10.9420	1.4e+01	27.9	20.8965	1.8e+00	-91.4
GW39-GW38	47.4718	1.1e+01	-76.8	12.6214	4.4e+00	-65.1
GW7-GW41	39.0234	1.5e+01	-61.6	12.9650	9.2e+00	-29.0
GW7-GW42	42.3530	1.3e+01	-69.3	18.3213	4.4e+00	-76.0





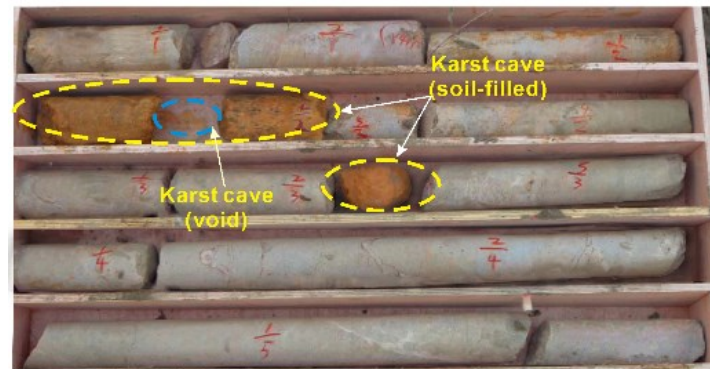
# Verification



Borehole YGW1

Depth (m)

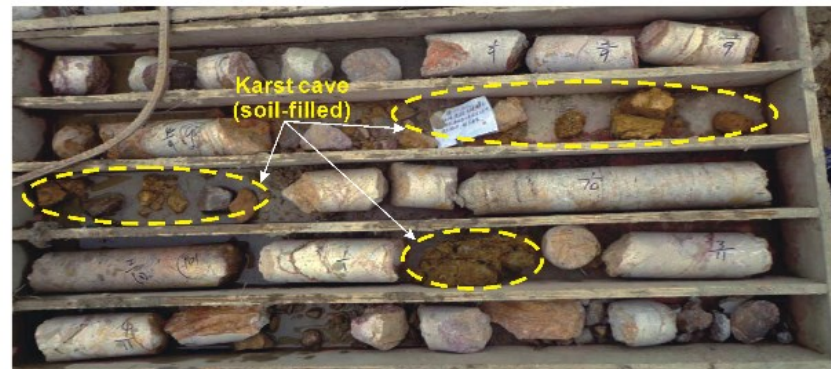
-85.7~ -87.7
-87.7~ -89.7
-89.7~ -91.7
-91.7~ -93.7
-93.7~ -95.7



Borehole YGW2

Depth (m)

-79.0~ -81.0
-81.0~ -83.0
-83.0~ -85.0
-85.0~ -87.0
-87.0~ -89.0



Borehole #	Property		Depth (m)		Coring rate (%)
	CT	Drilling	CT	Drilling	
YGW1	Karst cave (soil-filled)	Karst cave (soil-filled)	-87.74 to -89.09	-87.70 to -88.85	60-65
	Karst cave (void)	Karst cave (void)	-88.14 to -88.71	-88.10 to -88.70	50-60
	Karst cave (soil-filled)	Karst cave (soil-filled)	-90.73 to -91.16	-90.75 to -91.20	50-55
YGW2	Karst cave (soil-filled)	Karst cave (soil-filled)	-81.88 to -84.19	-81.80 to -83.90	60
	Karst cave (soil-filled)	Karst cave (soil-filled)	-86.59 to -86.87	-86.30 to -86.75	60



# Conclusions

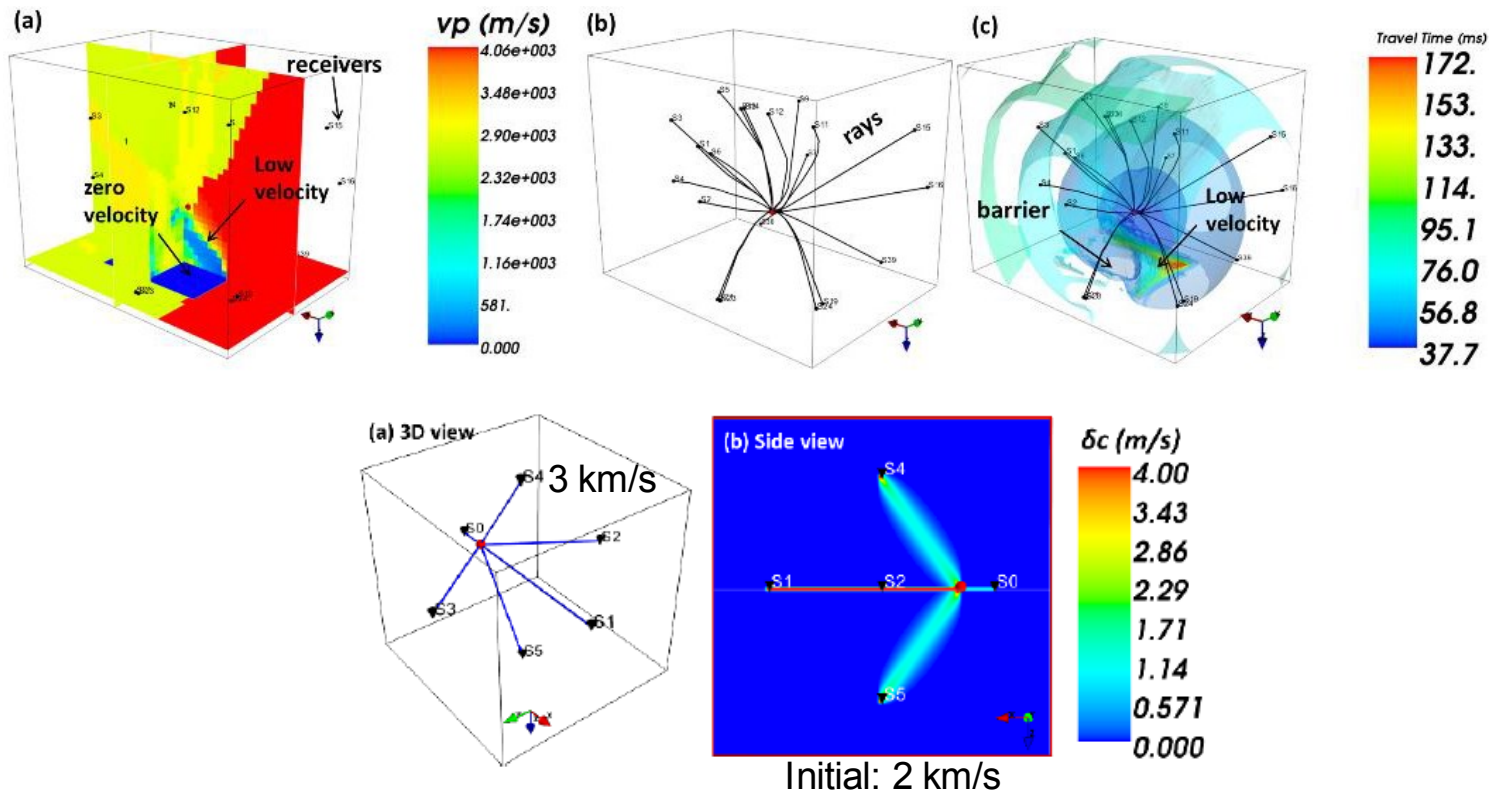


- Field test is performed to acquire seismic records with a depth more than 75 m.
- Data inversion methods are suggested to reconstruct caves through P-wave velocities.
- A quantitative basis for the interpretation of karst caves is provided.
- A real case is analyzed and the results are discussed.



# Perspectives

- Fast Sweeping Method (FSM) + Adjoint-state method  
(Huang and Bellefleur, 2012)



After Huang *et al.*, 2016



*Thank you*

## Cross-hole Seismic Field Experiments and Imaging for Karst Caves in Deep Foundations

Chenglong Duan\*, Changhong Yan, Baotian Xu, and Yinkang Zhou  
School of Earth Sciences and Engineering

Nanjing University, China

\*[clduan@itasca.cn](mailto:clduan@itasca.cn)